

## Randomly driven granular fluids: Large-scale structure

T. P. C. van Noije and M. H. Ernst

*Instituut voor Theoretische Fysica, Universiteit Utrecht, Postbus 80006, 3508 TA Utrecht, The Netherlands*

E. Trizac\* and I. Pagonabarraga

*FOM Institute for Atomic and Molecular Physics, Kruislaan 407, 1098 SJ Amsterdam, The Netherlands*

(Received 20 October 1998)

The nonequilibrium steady state of a granular fluid, driven by a random external force, is demonstrated to exhibit long-range correlations, which behave as  $\sim 1/r$  in three and  $\sim \ln(L/r)$  in two dimensions. We calculate the corresponding structure factors over the whole range of wave numbers, and find good agreement with two-dimensional molecular dynamics simulations. It is also shown by means of a mode coupling calculation, how the mean field values for the steady-state temperature and collision frequency, as obtained from the Enskog-Boltzmann equation, are renormalized by long wavelength hydrodynamic fluctuations.

[S1063-651X(99)03804-0]

PACS number(s): 81.05.Rm, 05.20.Dd, 05.40.-a

### I. INTRODUCTION

Systems of granular particles, like grains of sand or more ideally glass, plastic, or metal beads, exhibit different flow regimes [1], depending on the external forcing. A systematic experimental study of the rapid or collisional flow regime as compared to the quasistatic, slow, or frictional regime was first performed by Bagnold [2] using an annular shear cell. Later, a similar but more refined characterization was made in Ref. [3]. The possibility of coexistence of different flow regimes was observed in an experimental study of flows down an inclined chute [4].

In several more recent experimental studies of the *rapid granular flow* regime, more microscopic properties have been measured. In Ref. [5] the fluidization behavior of a vertically vibrated two-dimensional model granular material has been investigated using high-speed photography. Patterns at the surface of a vertically vibrated granular layer, analogous to Faraday waves in molecular fluids, have been observed in Ref. [6] and stimulated the interest of many theorists [7]. An understanding of these patterns through a derivation of, e.g., an amplitude equation [8] from the hydrodynamic description of the system, is still lacking, however. In Ref. [9] the effect of inelastic collisions on the formation of clusters is investigated in a system of particles rolling on a smooth surface and driven by a moving wall. Finally, Ref. [10] studies the steady state of a vertically shaken granular monolayer, and discusses clustering, inelastic collapse, and long-range order.

Even rapid flows of *model* granular materials are poorly understood in general, since complicating effects, such as gravity and interactions with boundaries, have to be taken into account. If the model granular material consists of spherical grains with a smooth surface, collisions between particles can be characterized only by their coefficient of

restitution  $\alpha$  or their inelasticity  $\epsilon = 1 - \alpha^2$ . We assume this coefficient of restitution to be a constant, independent of the relative velocity between the colliding particles, and refer to the model as the inelastic hard-sphere (IHS) model. Dissipative collisions complicate the dynamics in a nontrivial way: they may cause the system to become unstable, and give rise, for instance, to clustering; they create several new intrinsic length scales that might interfere for small inelasticity with the system size  $L$ , and for large inelasticity with the mean free path  $l_0$ .

By driving an IHS fluid by boundaries or external fields it can reach a steady or oscillatory state. Due to the existence of these new “cooling” lengths, this state is frequently inhomogeneous, where the spatial gradients become larger at higher inelasticity. Only for small inelasticity, the mean-free path is well separated from the scale on which the macroscopic fields vary, and a hydrodynamic description [11] through Navier-Stokes or Burnett equations is expected to hold. In fact, one of the primary goals in the study of rapid granular flows at *larger* inelasticities is to find the proper reduced set of macroscopic fields and the correct form of the relevant macroscopic continuum equations. The conceptual basis for the validity of the Navier-Stokes and Burnett equations of fluid dynamics in rapid granular flows breaks down due to the lack of scale separation. Therefore, we restrict ourselves mostly to small inelasticities, and explore the region of validity of the standard fluid dynamic description.

In the present paper we investigate the properties of an IHS fluid that is heated uniformly so that it reaches a spatially homogeneous steady state. This way of forcing, where a random external force accelerates a particle, was proposed by Williams and MacKintosh [12] for inelastic particles moving on a line. Peng and Ohta [13] performed simulations on a 2D version of this model. In two dimensions the model may be considered to describe the dynamics of light disks moving on an air table, a system that has been investigated experimentally in Ref. [14]. In three dimensions it can be extended to include gravitational and drag forces, making it to some extent relevant for gas-fluidized beds [15] when hydrodynamic interactions are unimportant. A similar IHS

---

\*Present address: Laboratoire de Physique Théorique et Hautes Energies, Bâtiment 211, Université Paris-Sud, 91405 Orsay Cedex, France.

model with random external accelerations has been used by Bizon and Swinney [16] in their computer simulations to test continuum theories for vertically vibrated layers of granular material.

In the present paper we will describe the randomly driven IHS fluid in two and three dimensions, and characterize its nonequilibrium steady state (NESS). The single-particle velocity distribution function in the NESS has been calculated in Ref. [17] from the Enskog-Boltzmann equation and was shown to be well approximated by a Maxwellian, except for an overpopulated tail  $\sim \exp(-Ac^{3/2})$ , where  $c$  is the velocity scaled by the thermal velocity and  $A \sim 1/\sqrt{\epsilon}$ . Computer simulations of the one-dimensional system of Ref. [12] showed the existence of long-range spatial correlations in the steady state, which were addressed theoretically in Ref. [18]. Here we will give quantitative predictions for long-range correlations [19] in the two- and three-dimensional NESS. Moreover, we extend the mode coupling theory of Brito and Ernst [20] to analyze how long wavelength fluctuations in the NESS renormalize the mean-field predictions of kinetic theory, and use this theory to calculate the renormalized temperature and collision frequency in the NESS.

To obtain an adequate description of the structures in steady granular flows, one does not only need the equations of fluid dynamics for the average macroscopic behavior, but also the spatial correlation functions  $G_{ab}(\mathbf{r})$ , and their Fourier transforms, the structure factors  $S_{ab}(\mathbf{k})$ . Let  $\delta a(\mathbf{r}, t) = a(\mathbf{r}, t) - \langle a(\mathbf{r}, t) \rangle$  with  $(a = n, T, u_\alpha)$  be the fluctuations of the slowly varying fields  $a(\mathbf{r}, t)$ , i.e., the local density  $n(\mathbf{r}, t)$ , local temperature  $T(\mathbf{r}, t)$ , and local flow velocity  $u_\alpha(\mathbf{r}, t)$  ( $\alpha = x, y, \dots$ ), around their average values  $\langle a(\mathbf{r}, t) \rangle$ . Then the objects of interest are the correlation functions in the NESS, which are given by the limit,

$$G_{ab}(\mathbf{r}) = \lim_{t \rightarrow \infty} \frac{1}{V} \int d\mathbf{r}' \langle \delta a(\mathbf{r} + \mathbf{r}', t) \delta b(\mathbf{r}', t) \rangle, \quad (1)$$

$$S_{ab}(\mathbf{k}) = \lim_{t \rightarrow \infty} V^{-1} \langle \delta a(\mathbf{k}, t) \delta b(-\mathbf{k}, t) \rangle.$$

Here  $\langle \dots \rangle$  is an average over some initial distribution,  $\delta a(\mathbf{k}, t)$  is the spatial Fourier transform of  $\delta a(\mathbf{r}, t)$ , and  $S_{ab}(\mathbf{k})$  is that of  $G_{ab}(\mathbf{r})$ . Moreover, we consider the unequal-time correlation functions in the NESS, defined as

$$F_{ab}(\mathbf{k}, t) = \lim_{t' \rightarrow \infty} V^{-1} \langle \delta a(\mathbf{k}, t' + t) \delta b(-\mathbf{k}, t') \rangle, \quad (2)$$

where  $F_{nn}(\mathbf{k}, t)$  is the *intermediate scattering function* [21]. The *dynamic structure factor* is then

$$S_{nn}(\mathbf{k}, \Omega) = \text{Re} \tilde{F}_{nn}(\mathbf{k}, z = i\Omega + 0), \quad (3)$$

where  $\tilde{F}_{ab}(\mathbf{k}, z)$  is the Laplace transform of  $F_{ab}(\mathbf{k}, t)$ .

The paper is organized as follows. In Sec. II we show how the macroscopic equations for granular flow are modified to account for the external driving/heating by the random accelerations. Section III characterizes the noise of external and internal fluctuations, and the structure factors and spatial correlation functions are calculated in Secs. IV and V. The latter section also presents the mode coupling calculations for the temperature and the collision frequency in the

NESS. Computational details of our molecular dynamics (MD) simulations are described in Sec. VI, and Sec. VII compares our predictions with simulations. Some general comments and conclusions are presented in Sec. VIII.

## II. MACROSCOPIC EQUATIONS

Consider a system of inelastic disks or spheres (IHS) ( $d = 2, 3$ ), driven by a heat source, which is described as a random acceleration  $\hat{\xi}_i$ ,

$$\frac{d\mathbf{v}_i}{dt} = \frac{\mathbf{F}_i}{m} + \hat{\xi}_i(t). \quad (4)$$

Here  $\mathbf{F}_i$  is the systematic force on particle  $i = (1, 2, \dots, N)$  due to inelastic collisions. If the time constant of the heat source is much smaller than the mean free time  $t_0$  between collisions, then  $\hat{\xi}_i(t)$  can be considered as Gaussian white noise with zero mean and correlation,

$$\overline{\hat{\xi}_{i\alpha}(t) \hat{\xi}_{j\beta}(t')} = \xi_0^2 \delta_{ij} \delta_{\alpha\beta} \delta(t - t'), \quad (5)$$

where  $\alpha, \beta = \{x, y, \dots\}$  denote Cartesian components of vectors or tensors. The overline indicates an average over the noise source. It is understood that the ensemble average in Eqs. (1) and (2), denoted by the angular brackets, also includes this noise average. To guarantee conservation of total momentum, the random force has to obey the constraint  $\sum_i \hat{\xi}_i(t) = \mathbf{0}$ . In thermodynamically large systems this constraint gives a correction to Eq. (5) of  $\mathcal{O}(1/N)$ , which can be neglected.

The uniformly heated fluid is described by the standard macroscopic equations of fluid dynamics, where the temperature equation is supplemented with an additional source term  $m\xi_0^2$ , and a sink term  $\Gamma$  to account, respectively, for the heating and the energy loss through inelastic collisions:

$$\partial_t n + \nabla \cdot (n\mathbf{u}) = 0,$$

$$\partial_t \mathbf{u} + \mathbf{u} \cdot \nabla \mathbf{u} = -\frac{1}{\rho} \nabla \cdot \mathbf{\Pi}, \quad (6)$$

$$\partial_t T + \mathbf{u} \cdot \nabla T = -\frac{2}{dn} (\nabla \cdot \mathbf{J} + \mathbf{\Pi} : \nabla \mathbf{u}) - \Gamma + m\xi_0^2,$$

where  $\rho = mn$ ,  $\mathbf{u}$  is the flow velocity, and  $\frac{1}{2} dnT$  is the kinetic-energy density in the local rest frame of the IHS fluid. The pressure tensor  $\mathbf{\Pi}_{\alpha\beta} = p\delta_{\alpha\beta} + \delta\mathbf{\Pi}_{\alpha\beta}$  contains the local pressure  $p$  and the dissipative momentum flux  $\delta\mathbf{\Pi}_{\alpha\beta}$ , which is proportional to  $\nabla_\alpha u_\beta$  and contains the kinematic and longitudinal viscosities  $\nu$  and  $\nu_l$ , defined below Eq. (A1) of Appendix A. The constitutive relation for the heat flux,  $\mathbf{J} = -\kappa \nabla T$ , defines the heat conductivity  $\kappa$ . For *small* inelasticity the transport coefficients  $\nu$ ,  $\nu_l$ , and  $\kappa$  are assumed to be given by the Enskog theory for a dense gas of elastic hard spheres (EHS) [22].

To lowest order in the spatial inhomogeneities, the sink term, representing the energy loss through inelastic collisions, is given by [23]

$$\Gamma = 2\gamma_0 \omega T. \quad (7)$$

It is proportional to the granular temperature, to the average Enskog collision frequency [ $\omega \sim \sqrt{T}$ , explicitly given in Eq. (A2) of Appendix A], and to the coefficient of inelasticity  $\epsilon = 1 - \alpha^2 \equiv 2d\gamma_0$ , where  $\alpha$  is the coefficient of normal restitution. To explain the term  $m\xi_0^2$  in Eqs. (6), we calculate the energy gain of a single particle due to the random force in a small time  $\delta t$ . This is done by formally integrating Eq. (4) and averaging over the noise source, i.e.,

$$\frac{1}{2}m[\overline{v_i^2(t+\delta t)} - \overline{v_i^2(t)}] = \frac{d}{2}m\xi_0^2 \delta t, \quad (8)$$

where Eq. (5) has been used. Note that we have defined the granular temperature as twice the average random kinetic energy per translational degree of freedom, so that the Boltzmann constant  $k_B$  does not appear in its definition.

The above equations provide a consistent description for the heated IHS fluid at small inelasticity. The energy is not conserved in inelastic collisions, and consequently, the temperature is *not* a hydrodynamic mode, but a kinetic mode with a relaxation rate  $\propto \gamma_0\omega$ . Nevertheless, at small inelasticities ( $\gamma_0 \ll 1$ ), it is consistent to include temperature among the slowly changing macroscopic variables, which describe the dynamics of the system on time scales  $t$  large compared to the mean free time  $t_0 = 1/\omega$ , and on spatial scales  $\lambda$  large compared to the mean free path,  $l_0 = v_0 t_0$ , where  $v_0 = \sqrt{2T/m}$  is the thermal velocity.

At large inelasticities, where  $\epsilon \sim \mathcal{O}(1)$ , we expect that the temperature is a *fast* kinetic mode, that decays on the time scale  $t_0$ , and cannot be included among the slow macroscopic variables. In that case, the IHS fluid becomes *athermal*, and the slow macroscopic fields only involve the density and flow field, as is the case in lattice gas cellular automata without energy conservation [24,25]. However, the proper constitutive relations for the IHS fluid at large inelasticities are not known.

Let us consider the decay of temperature in more detail. For a homogeneous state, the fluid dynamic equations (6) will have as a solution  $n(\mathbf{r},t) = n$ ,  $\mathbf{u}(\mathbf{r},t) = \mathbf{0}$ , and  $T(\mathbf{r},t) = T(t)$ , the latter satisfying

$$\partial_t T(t) = -\Gamma + m\xi_0^2. \quad (9)$$

For long times the system approaches a steady state with a constant temperature, determined by  $m\xi_0^2 = 2\gamma_0\omega T$ . As  $\omega \sim \sqrt{T}$ , we obtain the mean-field prediction [Eq. (A2)], as deduced from the Enskog theory,

$$T_E \equiv m \left( \frac{\xi_0^2 \sqrt{\pi}}{2\gamma_0 \Omega_d \chi n \sigma^{d-1}} \right)^{2/3}. \quad (10)$$

Further symbols are defined below [Eqs. (A1)] in the Appendix. To obtain the final approach to the NESS, we linearize Eq. (9) around  $T_E$  in Eq. (10). This yields an exponential approach, i.e.,

$$\delta T(t) \equiv T(t) - T_E = \delta T(0) \exp[-3\gamma_0\omega t]. \quad (11)$$

In fact,  $3\gamma_0\omega$  can be identified as the decay rate  $z_H(0)$  of the long wavelength components of the temperature fluctuations, as derived in Sec. IV below Eqs. (25). The exact time depen-

dent solution of Eq. (9) can be obtained implicitly ( $t$  as a function of temperature), and reads

$$f\left(\sqrt{\frac{T(t)}{T_E}}\right) - f\left(\sqrt{\frac{T_0}{T_E}}\right) = -\frac{3}{2} \frac{m\xi_0^2}{T_E} t, \quad (12)$$

where

$$f(x) = \ln|x-1| - \frac{1}{2} \ln(x^2+x+1) + \sqrt{3} \arctan\left(\frac{2x+1}{\sqrt{3}}\right). \quad (13)$$

and  $T_0$  is the temperature at  $t=0$ .

### III. NOISE CHARACTERISTICS IN THE NESS

The goal of this paper is to analyze the effects of spatial fluctuations  $\delta a(\mathbf{r},t)$  with ( $a = n, T, u_\alpha$ ) around the NESS on hydrodynamic space and time scales. As we are dealing with fluctuations, we linearize the nonlinear equations (6) around the NESS, with the result (A1) of Appendix A. Moreover, to extend the average equations to fluctuating equations, valid on mesoscopic spatial and temporal scales, we need to calculate the *external noise* terms  $\hat{\xi}^{\text{ex}}(\mathbf{r},t)$  and  $\hat{\theta}^{\text{ex}}(\mathbf{r},t)$  that contribute to  $\partial_t \mathbf{u}$  and  $\partial_t T$  in Eqs. (A1). These terms originate from the random acceleration  $\hat{\xi}_i(t)$ , which enters in the microscopic equations of motion (4). By starting from the microscopic expressions for the momentum and energy density, one finds that the noise sources are given by the *long* wavelength components of

$$\hat{\xi}^{\text{ex}}(\mathbf{r},t) = \frac{1}{n} \sum_i \hat{\xi}_i(t) \delta(\mathbf{r} - \mathbf{r}_i(t)), \quad (14)$$

$$\hat{\theta}^{\text{ex}}(\mathbf{r},t) = \frac{2m}{dn} \sum_i \mathbf{v}_i(t) \cdot \hat{\xi}_i(t) \delta(\mathbf{r} - \mathbf{r}_i(t)).$$

These fields are again Gaussian white noise with zero mean and correlations

$$\overline{\hat{\xi}_\alpha^{\text{ex}}(\mathbf{r},t) \hat{\xi}_\beta^{\text{ex}}(\mathbf{r}',t')} = \frac{1}{n} \xi_0^2 \delta_{\alpha\beta} \delta(\mathbf{r} - \mathbf{r}') \delta(t - t'), \quad (15)$$

$$\overline{\hat{\theta}^{\text{ex}}(\mathbf{r},t) \hat{\theta}^{\text{ex}}(\mathbf{r}',t')} = \frac{4mT}{dn} \xi_0^2 \delta(\mathbf{r} - \mathbf{r}') \delta(t - t'),$$

as follows from Eq. (5).

Next, we argue on the basis of the hydrodynamic equations (6) that there exists, close to the NESS, a range of hydrodynamic wave numbers  $k \gg k^*$ , the so-called *elastic regime*, where the dynamics of the fluctuations is the same as in a fluid of elastic hard spheres or disks, and is driven by *internal noise* that will be studied next. The validity of the hydrodynamic equations (6) and Eqs. (A1) is restricted to wave numbers  $k \ll 2\pi/l_0$  (to guarantee *separation* of kinetic and hydrodynamic scales), and to  $k \ll 2\pi/\sigma$ , where  $\sigma$  is the disk or sphere diameter (to guarantee that the Euler equations involve strictly *local* hydrodynamics). So, for the existence of an elastic regime in the IHS hydrodynamics, the following constraints must be satisfied:

$$k^* \ll k \ll \min\left\{\frac{2\pi}{l_0}, \frac{2\pi}{\sigma}\right\}. \quad (16)$$

Moreover, following McNamara [26] we can distinguish a *dissipative regime*,  $kl_0 \ll \epsilon$  [typically  $kl_0 \ll \mathcal{O}(\epsilon^2)$ ], and a *standard regime*,  $kl_0 \gg \epsilon$  [typically,  $kl_0 \gg \mathcal{O}(\sqrt{\epsilon})$ ], separated by a *crossover regime*, around  $kl_0 \sim \mathcal{O}(\epsilon)$ . In the dissipative regime, dissipation dominates compression effects and sound propagation, which are  $\mathcal{O}(kl_0)$ , as well as heat conduction, which is  $\mathcal{O}(k^2 l_0^2)$ . In the standard regime, dissipation effects are of the same order as heat conduction. As a consequence, the hydrodynamic modes and their propagation velocities are those of a fluid of *elastic* particles, while the corresponding damping rates of heat and sound modes still depend on the inelasticity. Only in the *elastic regime*,  $kl_0 \gg k^* l_0 \sim \mathcal{O}(\sqrt{\epsilon})$ ; also, these damping coefficients attain their elastic values. The above argument applies for small enough  $\epsilon = 1 - \alpha^2 = 2d\gamma_0$ , where the inequalities (16) are obeyed, and an elastic regime exists and is well separated from the dissipative regime.

In the *elastic regime* the equations for the macroscopic deviations from the NESS are the same as those for a fluid of *elastic* hard spheres, deviating from *thermal* equilibrium. To describe fluctuating mesoscopic hydrodynamics on these length scales, one can add *internal* noise  $\hat{\xi}^{\text{in}}(\mathbf{r}, t)$  and  $\hat{\theta}^{\text{in}}(\mathbf{r}, t)$ , describing the rapid microscopic degrees of freedom. The noise strength of the internal fluctuations can be obtained from the fluctuation-dissipation theorem [27,23] for the EHS fluid, and is given in Fourier representation by

$$\begin{aligned} V^{-1} \overline{\hat{\xi}_\alpha^{\text{in}}(\mathbf{k}, t) \hat{\xi}_\beta^{\text{in}}(-\mathbf{k}, t')} & \\ &= \frac{2T}{\rho} k^2 [\nu(\delta_{\alpha\beta} - \hat{k}_\alpha \hat{k}_\beta) + \nu_l \hat{k}_\alpha \hat{k}_\beta] \delta(t-t'), \\ V^{-1} \overline{\hat{\theta}^{\text{in}}(\mathbf{k}, t) \hat{\theta}^{\text{in}}(-\mathbf{k}, t')} &= \frac{8\kappa T^2}{d^2 n^2} k^2 \delta(t-t'), \end{aligned} \quad (17)$$

where  $\nu$ ,  $\nu_l$ , and  $\kappa$  are the transport coefficients for the EHS fluid, and  $\hat{k}_\alpha$  is a component of the unit vector  $\hat{\mathbf{k}} = \mathbf{k}/k$ . The *effective* noise in the heated IHS fluid may, therefore, be described by the sum of external and internal noise,  $\hat{\xi}(\mathbf{k}, t) = \hat{\xi}^{\text{ex}}(\mathbf{k}, t) + \hat{\xi}^{\text{in}}(\mathbf{k}, t)$ , with a similar expression for  $\hat{\theta}(\mathbf{k}, t)$ . The noise characteristics of  $\hat{\xi}(\mathbf{k}, t)$  and  $\hat{\theta}(\mathbf{k}, t)$  *interpolate* between two limiting behaviors and the corresponding noise strengths are given by the sum of Eqs. (15) and (17).

Having specified the characteristics of the noise sources in the macroscopic equations, we conclude this section by summarizing the Langevin-type equations that describe the dynamics of the slow fluctuations. To do so, it is convenient to introduce the Fourier modes  $\delta \mathbf{a}(\mathbf{k}, t) \exp[i\mathbf{k} \cdot \mathbf{r}]$  of the linearized hydrodynamic equations (A1). The mesoscopic equations, valid on hydrodynamic space and time scales, i.e.,  $t \gg t_0$  and  $kl_0 \ll 1$ , then take the form

$$\partial_t \delta \mathbf{a}(\mathbf{k}, t) = \mathbf{M}(\mathbf{k}) \delta \mathbf{a}(\mathbf{k}, t) + \hat{\mathbf{f}}(\mathbf{k}, t), \quad (18)$$

where the components of the vector  $\mathbf{a}$  are labeled with  $a = \{n, T, l, \perp\}$ . Here  $a = l$  refers to the longitudinal velocity

component  $u_l(\mathbf{k}, t) = \hat{\mathbf{k}} \cdot \mathbf{u}(\mathbf{k}, t)$ , and  $a = \perp$  refers to  $(d-1)$  transverse components of  $\mathbf{u}(\mathbf{k}, t)$ . The matrix  $M_{ab}$  with  $a, b = \{n, T, l, \perp\}$  is given explicitly in Eq. (A3), and  $\hat{f}_a(\mathbf{k}, t)$  is Gaussian white noise with *nonvanishing* components for  $a = T, l, \perp$  and correlation function

$$V^{-1} \overline{\hat{f}_a(\mathbf{k}, t) \hat{f}_b(-\mathbf{k}, t')} = C_{ab}(k) \delta(t-t'). \quad (19)$$

The noise strength  $C_{ab}(k) = \delta_{ab} C_{ab}(k)$  is obtained by taking the Fourier transform of Eqs. (15) together with Eqs. (17), and is only nonvanishing for the following diagonal elements:

$$\begin{aligned} C_{TT}(k) &= \frac{4mT\xi_0^2}{dn} + \frac{8\kappa T^2 k^2}{d^2 n^2} = \frac{4T\Gamma}{dn} + \frac{8\kappa T^2 k^2}{d^2 n^2}, \\ C_{ll}(k) &= \frac{\xi_0^2}{n} + \frac{2\nu_l T k^2}{\rho} = \frac{\Gamma}{\rho} + \frac{2\nu_l T k^2}{\rho}, \\ C_{\perp\perp}(k) &= \frac{\xi_0^2}{n} + \frac{2\nu T k^2}{\rho} = \frac{\Gamma}{\rho} + \frac{2\nu T k^2}{\rho}, \end{aligned} \quad (20)$$

where the NESS condition of Eq. (9), i.e.,  $\Gamma = 2\gamma_0 \omega T = m\xi_0^2$ , has been used.

#### IV. STRUCTURE FACTORS

The equal-time structure factors, introduced in Eqs. (1), obey the equations of motion,

$$\partial_t S_{ab}(\mathbf{k}) = \sum_c \{M_{ac}(\mathbf{k}) S_{cb}(\mathbf{k}) + M_{bc}(-\mathbf{k}) S_{ac}(\mathbf{k})\} + C_{ab}(k), \quad (21)$$

which follows by formally integrating Eq. (18) and using Eq. (19). The left-hand side of Eq. (21) vanishes since the structure factors do not depend on time in the NESS. The resulting equation can be solved by spectral analysis, or numerically. The spectral analysis is summarized in Appendix A, where  $w_{\lambda a}$  and  $v_{\lambda a}$  are, respectively, the  $a$ th component of the right and left eigenvectors of the hydrodynamic matrix  $\mathbf{M}$ , and  $z_\lambda(k)$  is the corresponding eigenvalue.

Taking then the scalar product of Eq. (21) on both sides with left eigenvectors (A5) of the Appendix, yields

$$\begin{aligned} \sum_{ab} \langle v_{\lambda a}(\mathbf{k}) | S_{ab}(\mathbf{k}) | v_{\mu b}(-\mathbf{k}) \rangle & \\ &= - \sum_{ab} \frac{\langle v_{\lambda a}(\mathbf{k}) | C_{ab}(k) | v_{\mu b}(-\mathbf{k}) \rangle}{z_\lambda(k) + z_\mu(k)}. \end{aligned} \quad (22)$$

Using the completeness relation (A6) and the fact that off diagonal elements of  $C_{ab}$  in Eqs. (20) vanish, we obtain

$$S_{ab}(\mathbf{k}) = - \sum_{\lambda\mu c} \frac{w_{\lambda a}(\mathbf{k}) v_{\lambda c}(\mathbf{k}) C_{cc}(k) v_{\mu c}(-\mathbf{k}) w_{\mu b}(-\mathbf{k})}{z_\lambda(k) + z_\mu(k)}, \quad (23)$$

which is the final result for the static structure factors. The time correlation function (2) in the NESS reduces in a similar manner to

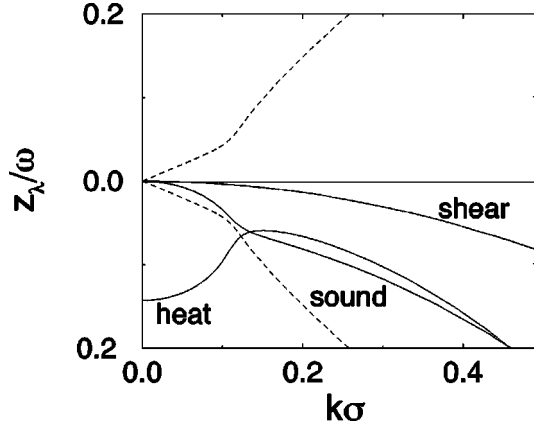


FIG. 1. Dispersion relations  $z_\lambda(k)/\omega$  versus  $k\sigma$  for  $\phi=0.4$ ,  $\alpha=0.9$ ; the solid lines refer to the real parts for  $\lambda=\perp, \pm$ , and  $H$ , respectively. Dashed lines represent the imaginary parts of the sound-mode relaxation rates ( $\lambda=\pm$ ). Here,  $l_0/\sigma \approx 0.34$ ,  $\gamma_0\sigma/l_0 \approx 0.14$ , and  $\sqrt{\gamma_0\sigma/l_0} \approx 0.64$ .

$$F_{ab}(\mathbf{k}, t) = \sum_{\lambda c} \exp[z_\lambda(\mathbf{k})t] w_{\lambda a}(\mathbf{k}) v_{\lambda c}(\mathbf{k}) S_{cb}(\mathbf{k}). \quad (24)$$

The above result corresponds to the Landau-Placzek theory [21] for hydrodynamic correlations in the NESS.

To obtain more explicit results we need the explicit forms of eigenvalues and eigenvectors, which have only been calculated for small  $k$ . The eigenvalue equation can be solved numerically for any given wave number, and the results are illustrated in Fig. 1 for the two-dimensional case. Transport coefficients, equation of state  $p(n, T)$ , and pair-correlation function at contact are obtained from Enskog's theory for *elastic* hard spheres or disks. The generic features of the spectrum in Fig. 1 are the same as McNamara's case " $\alpha = \beta = 0$ ," illustrated in Fig. 6(a) of his study [26] on hydrodynamics of granular materials, which corresponds to a temperature- and density-independent heat source. However, neither the equation of state, nor the transport coefficients, used in Ref. [26], correspond to the heated fluid of inelastic hard spheres, used in the present simulations. In the hydrodynamic regime ( $kl_0 \leq 1$ ), all eigenvalues are found to be *negative* for nonvanishing wave numbers (see Appendix A). So, all modes are linearly *stable*.

With the help of MATHEMATICA, the structure factors in the steady state have been calculated numerically from Eq. (21) with  $\partial_t S_{ab}(\mathbf{k}) = 0$  for a given wave number. The resulting structure factors are shown by solid lines in Fig. 2, and will be tested against MD simulations in Sec. VII.

Next, we present analytic results for the dissipative regime ( $kl_0 \ll \gamma_0$ ). The eigenvalues on the largest spatial scales can be determined as an expansion in powers of  $k$  at a fixed value of  $\gamma_0$ , with the results

$$\begin{aligned} z_\perp(k) &= -\nu k^2, \\ z_\pm(k) &= \mp ikv_D - D_S k^2, \\ z_H(k) &= -3\gamma_0\omega + D_H k^2. \end{aligned} \quad (25)$$

In later applications, the explicit form of the eigenvectors of  $\mathbf{M}(\mathbf{k})$  is needed to lowest order in  $\mathbf{k}$ . They read

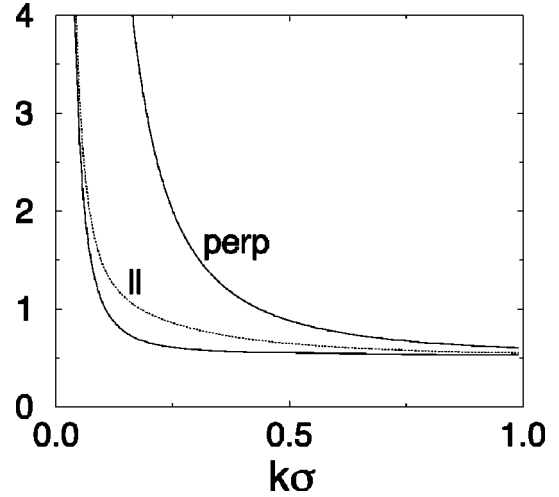


FIG. 2. Structure factors,  $S_\perp(k)$  and  $S_\parallel(k)$  in units  $T_0\sigma^2/m$ , as obtained from the full theory (solid lines) with external *and* internal noise. The dotted line represents  $S_\parallel^{\text{without}}(k)$  without internal noise with the plateau value added (see discussion at the end of Sec. VII). The parameters are  $\alpha=0.92$ ,  $\phi=0.63$ , and  $T_E=0.41T_0$ . Figure 6 shows that the  $S_\parallel$  simulation data agree much better with the solid line than with the dotted line.

$$\mathbf{w}_\perp(\mathbf{k}) = (0, 0, 0, 1), \quad \mathbf{v}_\perp(\mathbf{k}) = (0, 0, 0, 1),$$

$$\mathbf{w}_\pm(\mathbf{k}) = \frac{1}{\sqrt{2}} [1, -g(n)T/3n, \pm v_D/n, 0], \quad (26)$$

$$\mathbf{v}_\pm(\mathbf{k}) = \frac{1}{\sqrt{2}} (1, 0, \pm n/v_D, 0),$$

$$\mathbf{w}_H(\mathbf{k}) = (0, 1, 0, 0), \quad \mathbf{v}_H(\mathbf{k}) = (g(n)T/3n, 1, 0, 0).$$

The coefficients  $g(n)$ ,  $v_D$ , and  $D_\lambda$  with  $\lambda = \{\perp, H, \pm\}$  are calculated in the Appendix. In the dissipative regime there are two propagating sound modes ( $\lambda = \pm$ ) with a propagation speed  $v_D$  and a damping constant  $D_S$ . There is a *kinetic* heat mode ( $\lambda = H$ ), with a long wavelength relaxation rate  $z_H(0) = -3\gamma_0\omega$ , in agreement with Eq. (11). Therefore, on the largest spatial scales, the temperature deviations have decayed to zero, and temperature gradients do not exist; there is no heat conduction. In addition, there are  $(d-1)$  transverse velocity or shear modes ( $\lambda = \perp$ ), which are purely diffusive. The corresponding diffusivity,  $D_\perp = \nu$ , has the same form as for EHS. In Eqs. (A7)–(A10), the coefficients are expressed explicitly in terms of thermodynamic quantities and transport coefficients.

In the standard regime,  $kl_0 \gg \gamma_0$  (and  $\gamma_0$  small), the eigenvalues for shear and sound modes are to leading nonvanishing order the same as for the EHS fluid, where the sound waves propagate with the *adiabatic* sound speed  $v_S$  of the elastic fluid, which is larger than the propagation speed  $v_D$  in Eq. (A7). The damping of the sound and heat modes, on the other hand, are larger than in the elastic fluid due to the inelastic collisions. In the elastic regime, defined in Sec. III, where  $kl_0 \gg \sqrt{\gamma_0}$ , all transport coefficients are equal to their EHS values.

In summary, the eigenvalue spectrum  $z_\lambda(k)$  for the uniformly heated IHS fluid is quite different from that of the freely evolving IHS fluid, linearized around the homogeneous cooling state [26]. In the *free* case, all shear modes ( $\lambda = \perp$ ) and the heat mode ( $\lambda = H$ ) are unstable in the dissipative regime (small  $k$ ), and propagating modes do not exist for  $kl_0 \ll \gamma_0$ . Moreover, there exist in this regime a stable diffusive density mode and a kinetic temperature mode, which combine into two propagating modes for  $kl_0 \sim \mathcal{O}(\gamma_0)$ , where crossover occurs from the dissipative to the standard regime. In the *heated* case, however, all modes are linearly stable, and the sound modes remain propagating in the dissipative regime down to  $k=0$ .

## V. EFFECTS OF LONG-RANGE CORRELATIONS

In this section we study static and dynamic structure factors and corresponding correlation functions at the largest spatial scales. Moreover, we show by means of a mode coupling calculation, how average properties, which were calculated in Sec. II on the basis of a mean-field theory (i.e., the Enskog-Boltzmann equation), are renormalized by spatial fluctuations.

The static structure factors have been calculated in Eq. (23). In the *dissipative regime* ( $kl_0 \lesssim \gamma_0$ ), the relevant eigenvalues (25) and eigenmodes (26) are discussed below [Eq. (26)]. The dominant singularity at small wave number of the structure factors  $S_{ab}(k) \sim \mathcal{O}(1/k^2)$  in Eq. (23) originates from pairs of transverse modes, where  $2z_\perp(k) = -2\nu k^2$ , and from antiparallel sound modes, where  $z_+(k) + z_-(k) = -2D_S k^2$ . We start with the transverse structure factor, where only the shear modes in Eqs. (26) contribute, and deduce from the equations above,

$$S_\perp(k) \equiv S_{\perp\perp}(k) \approx \frac{\Gamma}{2\rho\nu k^2}, \quad (27)$$

where the relation (20) has been used for  $kl_0 \ll \gamma_0$ . The structure factors  $S_{ab}(k)$  for  $a, b \neq \perp$  derive their dominant small- $k$  behavior from two antiparallel sound modes and we obtain with the help of Eqs. (23), (25), (26), and (20) at small  $k$ ,

$$S_\parallel(k) \equiv S_{\parallel\parallel}(k) \approx \frac{\Gamma}{4\rho D_S k^2}, \quad (28)$$

where the sound damping constant in the dissipative regime  $D_S$  has been calculated in Eq. (A9). It depends on the inelasticity. The contribution of the internal noise is subdominant in this regime. In a similar manner, we find

$$S_{ab}(k) \approx B_{ab} S_{\parallel\parallel}(k) \quad (k \rightarrow 0), \quad (29)$$

where all nonvanishing coefficients labeled ( $ab$ ) = ( $ll, nn, TT, nT$ ) are listed in Table I. The remaining structure factors are of  $\mathcal{O}(1)$  as  $k \rightarrow 0$ .

Next, we consider the spatial correlation functions  $G_{ab}(r)$ , which are the inverse Fourier transforms of  $S_{ab}(k)$ . The small- $k$  behavior of  $S_{ab}(k)$ , obtained above, enables us to calculate the large- $r$  behavior of the spatial correlation

TABLE I. Coefficients  $B_{ab}$  in Eq. (29).

$ab$	$B_{ab}$
$ll$	1
$nn$	$n^2/v_D^2$
$TT$	$g^2(n)T^2/9v_D^2$
$nT$	$-g(n)nT/3v_D^2$

functions. The calculations are given in Appendix B. One finds for the leading large- $r$  behavior in *three-dimensional* systems,

$$G_\parallel(r) \approx \left( \frac{\Gamma}{8\pi\rho\nu} \right) \frac{1}{r}, \quad (30)$$

$$G_\perp(r) \approx \frac{\Gamma}{16\pi\rho} \left( \frac{1}{\nu} + \frac{1}{2D_S} \right) \frac{1}{r},$$

and in *two-dimensional* systems,

$$G_\parallel(r) \approx G_\perp(r) \approx \frac{\Gamma}{8\pi\rho} \left( \frac{1}{\nu} + \frac{1}{2D_S} \right) \ln\left(\frac{L}{r}\right), \quad (31)$$

valid for  $r \ll L$ , where  $L$  is the linear dimension of the system. The subleading large- $r$  corrections to Eq. (31) are constant terms, independent of  $r$ . In the calculations given in Appendix B, these constants depend on a cutoff wave vector  $k_{\min} = 2\pi/L$ , used to evaluate the divergent  $\mathbf{k}$  integrals occurring in the Fourier inversion of  $S_{ab}(k)$ . To calculate their precise values, the subleading small- $k$  corrections to Eqs. (27) and (28) are required.

The long wavelength behavior of the time-dependent correlation function  $F_{ab}(k, t)$  in Eq. (24) can be evaluated in a similar manner. We quote the result in terms of the Laplace transform  $\tilde{F}_{ab}(k, z)$ , from which the dynamic structure factor (3) follows. In the *dissipative regime* ( $kl_0 \ll \gamma_0$ ), we find to leading order for small wave numbers,

$$\tilde{F}_{\perp\perp}(k, z) \approx \frac{S_{\perp\perp}(k)}{z + \nu k^2}, \quad (32)$$

$$\tilde{F}_{\parallel\parallel}(k, z) \approx \frac{1}{2} \sum_{\lambda=\pm} \frac{S_{\parallel\parallel}(k)}{z + i\lambda k v_D + D_S k^2}.$$

In a similar manner we obtain

$$\tilde{F}_{ab}(k, z) \approx B_{ab} \tilde{F}_{\parallel\parallel}(k, z), \quad (33)$$

where all nonvanishing coefficients  $B_{ab}$  are listed in Table I. The dynamic structure factor (3) then becomes

$$S_{nn}(k, \Omega) \approx \frac{1}{2} \sum_{\lambda=\pm} \frac{D_S k^2 S_{nn}(k)}{(\Omega + \lambda k v_D)^2 + D_S^2 k^4}. \quad (34)$$

It contains only Brillouin peaks, coming from the sound modes. There is no central Rayleigh peak, because the heat mode is not a slow, but a fast kinetic mode in this regime. In the elastic regime,  $S_{nn}(k, \Omega)$  has the standard Rayleigh and Brillouin lines of the EHS fluid.

The existence of long-range spatial correlations shows that the NESS is quite different from a thermal equilibrium state [19]. In fact, the spatial fluctuations also modify (renormalize) the mean-field predictions for the averages and the particle distribution functions. In Appendix C a mode coupling calculation is presented to estimate the renormalization effects on the average energy per particle  $E = (1/N)\sum_i \langle \frac{1}{2} m v_i^2 \rangle$  and average collision frequency  $\omega$  in the NESS, and we recall their mean-field values, i.e.,  $E_E = \frac{1}{2} d T_E$  and  $\omega_E$  given by Eq. (A2), i.e.,  $\omega_E \propto n \chi(n) \sqrt{T_E}$ , where  $T_E$  is given in Eq. (10).

As it turns out, the fluctuation contributions,  $\delta E$  and  $\delta \omega$ , are finite and well-behaved in *three* dimensions, but logarithmically divergent in the system size  $L$  in *two* dimensions, so that  $d=2$  is the upper critical dimension. The mode coupling calculations of Appendix C yield then in two dimensions, for large  $L$ ,

$$\begin{aligned} T_{\text{NESS}} &\approx T_E + \frac{C_E}{4\pi} \ln\left(\frac{\gamma_0 L}{l_0}\right), \\ \omega_{\text{NESS}} &\approx \omega_E + \frac{C_\omega}{4\pi} \ln\left(\frac{\gamma_0 L}{l_0}\right), \end{aligned} \quad (35)$$

where  $C_E$  and  $C_\omega$  are calculated in Appendix C. The argument of the logarithm  $\gamma_0 L/l_0$  is an estimate for the ratio of the values for the right ( $k \sim \gamma_0/l_0$ ) and left ( $k_{\min} = 2\pi/L$ ) boundaries of the dissipative  $k$  range, where the small- $k$  behavior in Eqs. (27) to (29) is valid. The logarithmic correction becomes only appreciable for large systems with a size  $L$ , much larger than the so-called homogeneous cooling length  $l_T = l_0/\gamma_0$ , which diverges in the elastic limit. Then the renormalization corrections for small inelasticity vanish as  $\delta T \sim \epsilon \ln(\epsilon L/l_0)$  and  $\delta \omega \sim \epsilon^2 \ln(\epsilon L/l_0)$ . Here, we have used the relations  $C_E \sim \epsilon$  and  $C_\omega \sim \epsilon^2$  for  $\epsilon \rightarrow 0$ , as can be deduced from the results in Appendix C. A similar mode coupling theory has been recently used in Ref. [20] for freely evolving granular fluids to calculate the long-time decay of the energy, which deviates from Haff's cooling law due to inhomogeneities in the hydrodynamic fields, and good agreement between theory and simulations was found.

Before concluding this section, we compare the theoretical predictions for the structure factors, with and without internal noise in Eqs. (20) and (21), as shown in Fig. 2. Inspection of Eqs. (27) and (28) shows that only the external noise determines their dominant small- $k$  behavior. The question then arises, what are the effects of internal noise, and is it meaningful to include it in the theoretical description? The answer is affirmative, as we will show below. The steady state solution of Eq. (21) *without internal noise* clearly behaves at small wave numbers as  $k^{-2}$ , but the  $k$ -independent plateau values, shown by the full theory (solid lines in Fig. 2), are missing. These plateau values represent a very short-distance correlation  $\sim \delta(\mathbf{r})$ . Calculation of the plateau value for  $S_{\alpha\beta}(\mathbf{k})$  yields  $(1/n^2 V) \langle \sum_i v_{i\alpha} v_{i\beta} \rangle = (T/\rho) \delta_{\alpha\beta}$ , i.e., the self-correlation term ( $i=j$ ) in the definition (1) of  $S_{\alpha\beta}(\mathbf{k})$ , or more explicitly in Eq. (40) below. Then, addition of this plateau value to the numerical solution of Eq. (21) *without internal noise* yields the structure factors  $S_{\alpha\beta}^{\text{without}}(\mathbf{k})$ , shown as dotted lines in Fig. 2. For the transverse velocity structure

factor, the dotted line coincides with the solid line in Fig. 2, as can be shown analytically from Eqs. (20) and (21). Only the structure factor for the longitudinal flow field,  $S_{\parallel}^{\text{without}}(k)$  differs appreciably from  $S_{\parallel}(k)$  in the relevant intermediate regime,  $0.2 \leq k\sigma \leq 0.5$ .

In Sec. VII the simulation results will be compared with the theoretical predictions with and without internal noise. As it turns out, the comparison shows convincingly that the theory with/without internal noise agrees/disagrees with the simulations.

## VI. COMPUTATIONAL DETAILS

In the two subsequent sections we describe molecular dynamics simulations performed to verify our theoretical predictions. In this section we present the computational details, before testing our theoretical results against simulations in the next section.

The model studied here has been extensively used in computer simulations for the freely evolving case (no forcing) [28–30,23], as well as for the randomly accelerated case in one [12] and two dimensions [13]. We consider a system of  $N$  inelastic hard disks having diameter  $\sigma$  in a two-dimensional square cell of length  $L$ , with periodic boundary conditions. The disks interact via inelastic collisions with coefficient of normal restitution  $\alpha$ . For a colliding pair ( $i, j$ ) of particles having equal masses, the postcollision velocities are:

$$\begin{aligned} \mathbf{v}_i^* &= \mathbf{v}_i - \frac{1}{2}(1+\alpha)(\mathbf{v}_{ij} \cdot \hat{\boldsymbol{\sigma}}) \hat{\boldsymbol{\sigma}}, \\ \mathbf{v}_j^* &= \mathbf{v}_j + \frac{1}{2}(1+\alpha)(\mathbf{v}_{ij} \cdot \hat{\boldsymbol{\sigma}}) \hat{\boldsymbol{\sigma}}, \end{aligned} \quad (36)$$

where  $\mathbf{v}_{ij} = \mathbf{v}_i - \mathbf{v}_j$ , the asterisk denotes velocities after collision, and  $\hat{\boldsymbol{\sigma}}$  is a unit vector along the line connecting the centers of particle  $j$  and particle  $i$ .

The energy loss in consecutive collisions, which is proportional to  $\epsilon = 1 - \alpha^2$ , is compensated by a periodic (in time) and instantaneous perturbation of all velocities by a random amount. After every time step  $\Delta t$ , the velocity of each particle is modified according to

$$\mathbf{v}_i \rightarrow \mathbf{v}_i + \boldsymbol{\varphi}_i, \quad 1 \leq i \leq N, \quad (37)$$

where the components of the vectors  $\boldsymbol{\varphi}_i$  are taken from a random distribution of zero mean and variance  $\varphi_0$  (in practice, a Gaussian or a flat function of finite support). The time step  $\Delta t$  of this ‘‘heating’’ or ‘‘kicking’’ is chosen much smaller than the mean time between successive collisions of a tagged particle (typically a factor  $10^4$  smaller), so that the system under scrutiny reduces to that described in Sec. II. The opposite limit, where  $\Delta t$  is much bigger or comparable to the mean-free path, was considered in Ref. [31] (in the presence of an additional external damping or drag force), and in that limit, clustering was observed. The relation between  $\varphi_0$  and  $\xi_0$ , the variance of the noise term in Eq. (4), can be deduced from the energy fed into the system by the kicks. This yields straightforwardly,

$$\xi_0^2 = \frac{\varphi_0^2}{\Delta t}. \quad (38)$$

Between the heating events, the motion of the disks is free, which enables us to implement an event-driven molecular dynamics scheme with a linked-list method [32]. The CPU time, however, scales like  $N^2$  because the lists in all cells need to be updated after each heating event.

Four parameters determine the state of the system: the inelasticity  $\epsilon = 1 - \alpha^2$ , the packing fraction  $\phi = \pi N \sigma^2 / (4L^2)$ , the reduced lower wave number cutoff  $k_{\min} \sigma = 2\pi \sigma / L$ , and the heating rate  $\xi_0^2$ . The values of  $N$  investigated in this article vary between  $10^3$  and  $10^4$ , and we shall restrict our attention to high packing fractions for which the use of linked lists implies the most significant reduction of computer time. We consider the cases of moderate inelasticities ( $0.6 < \alpha < 1$ ) and complete inelasticity ( $\alpha = 0$ ). For the latter case, inelastic collapse occurs, i.e., the collision frequency involving only a small number of correlated particles diverges, as observed first by McNamara and Young [29] in freely evolving fluids of inelastic hard disks. Also in our system, for high enough inelasticity, the heating seems never sufficient to prevent the inelastic collapse. For  $\alpha < 0.5$ , the inelastic collapse has been avoided by introducing a slight modification of collision rule (36), as proposed in [30]: in each collision, the velocities are first computed according to the standard procedure  $(\mathbf{v}_1, \mathbf{v}_2) \rightarrow (\mathbf{v}_1^*, \mathbf{v}_2^*)$ ; the relative velocity  $\mathbf{v}_{12}^*$  is then rotated by a random angle smaller than a maximum value  $\Theta$  (typically less than a few degrees), keeping the center-of-mass velocity fixed. Note that this modified collision rule does not change the total energy loss of the colliding pair, and does not introduce any spurious drag or forcing on the particles.

The structure factors in the NESS have been computed for wave vectors compatible with the periodic boundary conditions, i.e., of the form  $(2\pi/L)(n_x, n_y)$ . We have obtained the density-density structure factors,

$$\begin{aligned} S_{nn}(\mathbf{k}) &= \frac{1}{V} \left\langle \left| \sum_{i,j} \exp(-i\mathbf{k} \cdot \mathbf{r}_{ij}) \right|^2 \right\rangle \\ &= \frac{1}{V} \left\langle \left| \sum_i \exp(-i\mathbf{k} \cdot \mathbf{r}_i) \right|^2 \right\rangle, \end{aligned} \quad (39)$$

and the velocity-velocity structure factor, defined as

$$n^2 S_{\alpha\beta}(\mathbf{k}) = \frac{1}{V} \left\langle \sum_{i,j} v_{i\alpha} v_{j\beta} \exp(-i\mathbf{k} \cdot \mathbf{r}_{ij}) \right\rangle. \quad (40)$$

Here, the averages are taken in the spatially uniform NESS. The fluctuation  $\delta g_\alpha$  in the momentum density,  $\delta g_\alpha(\mathbf{k}) = \sum_i m v_{i\alpha} \exp(-i\mathbf{k} \cdot \mathbf{r}_i)$ , and those in the flow field are related as  $\delta g_\alpha = \rho \delta u_\alpha$ , where  $\rho$  is the average mass density in the steady state. The second rank tensor  $S_{\alpha\beta}(\mathbf{k})$  is isotropic and can be split into a longitudinal and transverse part,

$$S_{\alpha\beta}(\mathbf{k}) = \hat{k}_\alpha \hat{k}_\beta S_{\parallel}(k) + (\delta_{\alpha\beta} - \hat{k}_\alpha \hat{k}_\beta) S_{\perp}(k), \quad (41)$$

where  $\hat{k} = \mathbf{k}/k$ . From Eq. (39), it appears that the knowledge of  $S_{nn}$  requires the computation of an  $\mathcal{O}(N)$  quantity. We can rewrite the velocity-velocity structure factor so that its computation also increases linearly with the number of particles. For example, for the longitudinal part of  $S_{\alpha\beta}(\mathbf{k})$  in Eq. (41) we have,

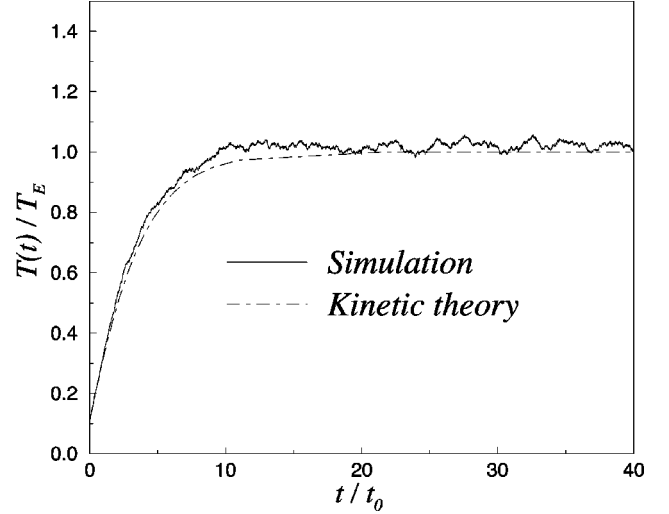


FIG. 3. Granular temperature as a function of time for  $\alpha = 0.92, \phi = 0.078$  ( $l_0/\sigma \approx 3.5$ ), and  $N = 1600$  particles. The simulation result is compared to the analytical expression (12) (dashed curve). The initial condition corresponds to a fluidlike configuration of elastic hard disks. Here  $\Delta t = 3.8 \times 10^{-3} (m\sigma^2/T_0)^{1/2} \approx 1.5 \times 10^{-3} t_0$  and  $\varphi_0 = 5.77 \times 10^{-2} (T_0/m)^{1/2}$ .  $T_E$  is the temperature expected on the basis of the Enskog theory [see Eq. (10)]. For the above parameters, there are on average 3.7 collisions per time interval  $\Delta t$  in the NESS, and  $T_E/T_0 = 9.3$ .

$$n^2 S_{\parallel}(k) = \frac{1}{V} \left\langle \left| \sum_i (\mathbf{v}_i \cdot \hat{\mathbf{k}}) \exp(-i\mathbf{k} \cdot \mathbf{r}_i) \right|^2 \right\rangle. \quad (42)$$

In practice, the different  $S_{aa}(k)$  have been computed for every  $\mathbf{k}$  lying in the disk  $|\mathbf{k}| < k_{\max} = 6\pi/\sigma$ , then averaged over shells of thickness  $k_{\min} = 2\pi/L$ , to achieve better accuracy. Moreover, the statistics in the NESS has been increased by averaging over time. Note that the above procedure, which gives insight into the microscopic to large scale structure of the system, does not require the knowledge of the hydrodynamic (coarse-grained) density and velocity fields.

## VII. SIMULATION RESULTS

### A. Approach and characterization of the NESS

Before addressing the question of the large scale structure of the inelastic fluid, we investigate the validity of the macroscopic description given in Secs. II and V. The former section gives the mean-field results for the steady-state temperature  $T_E$  in Eq. (10) and collision frequency  $\omega_E$  in Eq. (A2), based on the Enskog-Boltzmann equation. The latter section and Appendix C show how the long-range spatial fluctuations renormalize these mean-field values and lead to estimates in Eqs. (35) for the corrections  $\delta T = T - T_E$  and  $\delta \omega = \omega - \omega_E$ , using a mode coupling calculation.

When the system is initially prepared in a configuration having a temperature  $T_0$  different from the steady-state temperature  $T_E$ , the time dependence predicted by the mean-field result (12) is in good agreement with the numerical data. This is shown in Fig. 3 for a system with small inelasticity. When the initial temperature  $T_0$  is much larger than  $T_E$ , the heating at short times is dominated by the inelastic dissipation, and Eq. (12) becomes Haff's homogeneous cool-

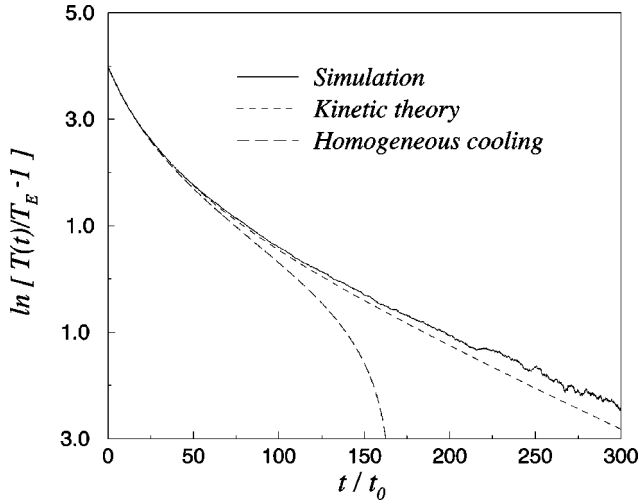


FIG. 4. Time dependence of the granular temperature obtained in the simulation for the two-dimensional system of Fig. 3, with  $\Delta t = 3.8 \times 10^{-2} (m\sigma^2/T_0)^{1/2}$ ,  $\varphi_0 = 1.7 \times 10^{-3} (T_0/m)^{1/2}$ . Comparison is made with Haff's law (43) for homogeneous cooling (dashed curve), and with the full solution of Eq. (12) (long-dashed curve). Here,  $T_E/T_0 = 0.018$ .

ing law for a freely evolving system,

$$\frac{T(t)}{T_0} = \frac{1}{(1 + \gamma_0 t/t_0)^2}, \quad (43)$$

where  $t_0 = 1/\omega_E(T_0)$  is the mean-free time in the initial state. This can be seen from the asymptotic expansion of the function  $f$  defined in Eq. (13),

$$f(x) \simeq \sqrt{3} \frac{\pi}{2} - \frac{3}{x} \quad \text{for } x \rightarrow \infty. \quad (44)$$

These analytic results for short times are confirmed by MD simulations, as shown in Fig. 4. Moreover, for initial temperatures  $T_0 \ll T_E$ , Eq. (12) predicts at short times a linear increase of  $T$ , as in a heated fluid of elastic hard spheres. Our simulations confirm this behavior.

Figure 5 shows that the measured kinetic energy per particle  $T$  is larger than the temperature  $T_E$  predicted on the basis of mean-field theory. This effect is noticeable albeit small in the results reported in Figs. 3 and 4, which correspond to the nearly elastic limit. For the densities studied here, we observe (see Fig. 5) that the correction  $\delta T$  is positive and decreases with decreasing inelasticity. The positive excess in temperature is already present for small inelasticity (see, e.g., Fig. 4), and vanishes as  $\epsilon \rightarrow 0$ . Note that the above results are at variance with those reported by Peng and Ohta [13], who find that  $T/T_E$  does not depend on  $\alpha$ . The measured collision frequency  $\omega$  is also larger than the Enskog estimate  $\omega_E$ , as shown in Fig. 5. The excess  $\delta\omega$  increases with increasing inelasticity.

We first observe that the simulation data in Fig. 5, where both  $\omega > \omega_E$  and  $T > T_E$ , cannot be explained consistently as a possible over or underestimation of the IHS pair correlation function  $\chi_{\text{IHS}}$  at contact by its value for elastic disks. On the basis of Eqs. (10) and (A2), we note that an overestimation of  $\chi_{\text{IHS}}$  would increase the collision frequency (A2), and

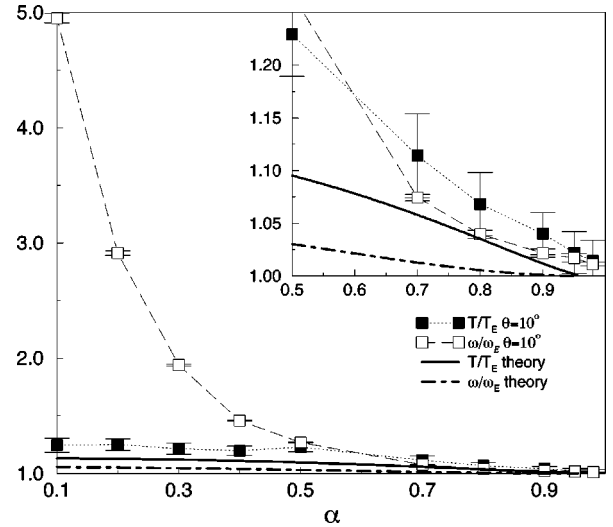


FIG. 5. Measured excess temperature  $\delta T = T - T_E$  and collision frequency  $\delta\omega = \omega - \omega_E$  versus coefficient of restitution  $\alpha$ , for  $L = 60\sigma$ ,  $N = 917$  ( $\phi = 0.2$ ,  $l_0 = 1.1\sigma$ ), and a maximal random rotation angle  $\Theta = 10^\circ$ , together with the predictions of the mode coupling theory, Eq. (35).

decrease the temperature (10). These trends are at variance with the observations. The discrepancy between the measured and predicted temperatures and collision frequencies is more likely due to large scale fluctuations, at least for not too large inelasticities ( $\alpha \gtrsim 0.6$ ). These long-range spatial fluctuations renormalize the mean-field Enskog values for the temperature  $T_E$  and collision frequency  $\omega_E$  by amounts  $\delta T$  and  $\delta\omega$ . The theoretical estimates (35), based on mode coupling arguments, show the correct trends for the dependence of these corrections on the inelasticity, i.e.,  $\delta T \sim \epsilon$  and  $\delta\omega \sim \epsilon^2$  as  $\epsilon \rightarrow 0$ , and give a rough estimate of the magnitude of these terms as illustrated in the inset of Fig. 5. We also point out that the system size considered in Fig. 5 is much too small for the asymptotic theory (35) to be applicable. For instance, at  $\alpha = 0.8$ , we deduce from the data ( $l_0 = 1.1\sigma$ ,  $L = 60\sigma$ ) in the caption of Fig. 5 that  $\gamma_0 L/l_0 \approx 4.9$ . Consequently, the leading asymptotic term  $\ln(\gamma_0 L/l_0) \approx 1.6$  does not dominate the full mode coupling contribution (C2) in Appendix C, where subleading terms of  $\mathcal{O}(1)$  have been neglected. The corresponding ratios  $\gamma_0 L/l_0$  for Figs. 6 ( $\alpha = 0.92$ ), 8 ( $\alpha = 0.6$ ), and 11 ( $\alpha = 0$ ) are, respectively, 46, 127, and 297. This predicts for the systems in Figs. 6, 8, and 11, respectively,  $T_{\text{NESS}}/T_E \approx 1.07$ , 1.41, and 1.77, whereas the simulations yield for the observed values  $T/T_E \approx 1.05$ , 1.45, and 1.5, which agrees quite well. The good agreement at  $\alpha = 0$  is unexpected, as the theory is constructed under conditions that apply at small inelasticity. However, the renormalized values for the collision frequency, as predicted by the mode coupling theory, are much too small. We find in the above Figs. 6, 8, and 11, respectively, for the theoretical values  $\omega_{\text{NESS}}/\omega_E \approx 1.003$ , 1.06, and 1.12, whereas the simulations yield  $\omega/\omega_E \approx 1.05$ , 1.36, and 22.9.

For large inelasticity ( $\alpha < 0.5$ ), the temperature  $T$  and collision frequency  $\omega$  depend on the maximum angle  $\Theta$  of the random rotations, used to avoid the collapse singularity, as explained in Sec. VI. In fact,  $\omega$  diverges at  $\Theta = 0$  (inelastic collapse), in agreement with the observations of Peng and

TABLE II. Collision frequency (normalized by the Enskog value) as a function of  $\Theta$ , for a totally inelastic system ( $\alpha=0$ ) with  $N=1600$  particles, and packing fraction  $\phi=0.07$ .

$\Theta$	$1.5^\circ$	$3.5^\circ$	$5^\circ$	$45^\circ$	$90^\circ$
$\omega/\omega_E$	8.2	7.4	7	4.3	4.3

Ohta [13]. Intuitively, one expects that a *larger* randomization of the postcollision velocities (larger  $\Theta$ ) more effectively destroys the correlations leading to inelastic collapse, and consequently *decreases* the deviations in  $T$  and  $\omega$  from the mean field and the mode coupling predictions. This does happen indeed for both temperature and collision frequency, as can be seen from Table II.

### B. Fluctuations in the NESS

In this section we analyze the effects of inelasticity on the large distance behavior of the fluid. We have computed the structure factors in the spatially homogeneous NESS of the inelastic hard disk fluid as explained in the previous section, and have focused either on values of  $\alpha$  close to the elastic limit, where the theoretical description is supposed to apply, or on values close to 0, in order to test how large deviations from the theory might be. Local mean-field values, like  $T_E$  and  $\omega_E$ , reach their steady-state values rapidly. However, the time scale needed for the structure factors  $S_{ab}(\mathbf{k})$  and the contributions of spatial fluctuations,  $\delta T$  and  $\delta\omega$ , to reach their steady-state values are diffusive, and increase as  $k_{\min}^{-2} \sim L^2$  with system size. We have checked in the simulations

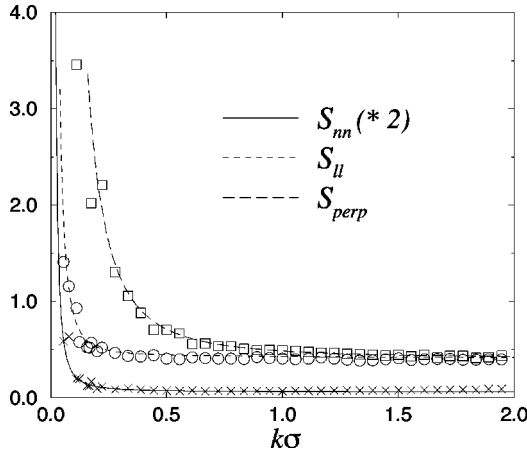


FIG. 6. Structure factors  $S_{\perp}$  and  $S_{\parallel}$  (in units  $T_0\sigma^2/m$ ) and  $S_{nn}$  (in units  $1/\sigma^2$ ) versus wave vector for  $\alpha=0.92$ ,  $\phi=0.63$  ( $l_0/\sigma \approx 0.095$ ), and  $N=10201$ . The noise strength is chosen such that  $T_E=0.41T_0$ . The simulation data (symbols) have been averaged over  $10^2$  successive configurations, separated by a time interval of 20 collisions per particle.  $S_{\parallel}$  and  $S_{perp} \equiv S_{\perp}$  are, respectively, the parallel and perpendicular parts of the velocity-velocity structure factor, defined by Eq. (40). Comparison is made with the theoretical expressions (full, dashed, and long-dashed curves) deduced from Eq. (23) (compare also Fig. 2). There is a dissipative regime for  $k\sigma \lesssim \gamma_0\sigma/l_0 \approx 0.40$ , and an elastic regime for  $k\sigma \gtrsim \sqrt{\gamma_0}\sigma/l_0 \approx 2.1$ . Here,  $T/T_E \approx \omega/\omega_E \approx 1.05$ , whereas the mode coupling approach of Sec. V predicts  $T_{NESS}/T_E \approx 1.07$  and  $\omega_{NESS}/\omega_E \approx 1.003$ .

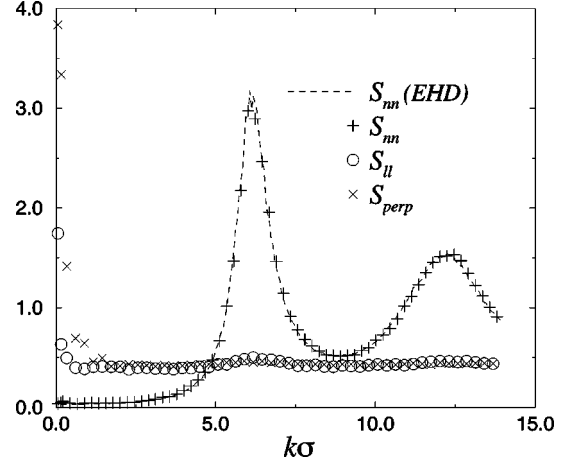


FIG. 7. Same as Fig. 6, with  $k$  beyond the dissipative regime. The dashed curve corresponds to the density-density structure factor of an elastic hard disk system of the same size and packing fraction (dashed curve). All results are deduced from MD simulations.

that the large scale behavior of the structure factors was properly equilibrated before accumulating the data used to compute the averages.

First of all, we have tested the isotropy of tensor (40) by checking that the average,

$$\left\langle \sum_{i,j} (\mathbf{v}_i \cdot \hat{\mathbf{k}})(\mathbf{v}_j \cdot \hat{\mathbf{k}}_{\perp}) \exp(i\mathbf{k} \cdot \mathbf{r}_{ij}) \right\rangle, \quad \text{with } \hat{\mathbf{k}} \cdot \hat{\mathbf{k}}_{\perp} = 0, \quad (45)$$

vanishes for  $\mathbf{k}$  values compatible with the periodic boundary conditions.

In Fig. 6 we show the density-density structure factor and the relevant components of the velocity-velocity structure factors. For *elastic* hard disks the plateau values of  $S_{aa}(k)$  around  $k\sigma \approx 2$  extend all the way down to  $k=0$ . The excess correlations in the dissipative regime ( $k \lesssim \gamma_0/l_0$ ), which for  $S_{\perp}(k)$  extend up to  $k \approx \sqrt{\gamma_0}/l_0$ , are characteristic of the randomly driven inelastic fluid. Figure 6 shows that for small inelasticities the agreement between simulations and theory is quite reasonable. The structure factors diverge at small scales like  $k^{-2}$ , in agreement with the theoretical predictions (27)–(29). The packing fraction has been chosen fairly high ( $\phi=0.63$ ) but lower than the two-dimensional random close packing of monodisperse disks  $\phi_{RCP} \approx 0.82$  [33], and inside the *liquid* region of the phase diagram for elastic hard disks. In addition to the gain in computer time, such a packing fraction leads to a mean-free-path  $l_0$  smaller than the particle diameter  $\sigma$  (e.g.,  $l_0 \approx 0.095\sigma$  for  $\phi=0.63$ ). Therefore, the hydrodynamic regime will hold up to typical particle diameters, enlarging the range of wave vectors where comparison between simulations and theoretical predictions is feasible. Moreover, for dense systems, a marked density structure is to be expected at the molecular scale, especially at wavelengths close to  $\sigma$  ( $k\sigma \approx 2\pi$ ). Figure 7 shows that for  $\alpha$  close to 1, this structure is indistinguishable from the structure for elastic hard disks. Note that  $S_{\parallel}(k)$  and  $S_{\perp}(k)$ , although quite structureless for  $k\sigma > 1$ , show a weak and broad peak correlated with the maximum of  $S_{nn}(k)$ . This feature is more pronounced as the inelasticity increases, as shown in Figs. 10

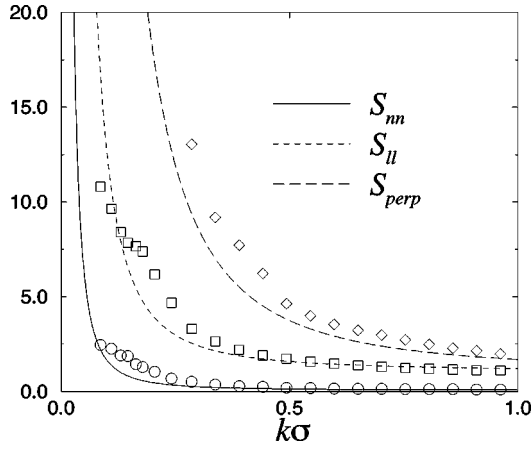


FIG. 8. Structure factors for  $\alpha=0.6$ ,  $\phi=0.55$  ( $l_0/\sigma \approx 0.15$ ),  $N=10201$ , and  $T_E=1.0T_0$ . The lines are the corresponding theoretical predictions. The measured temperature  $T/T_E \approx 1.45$  and our mode coupling theory gives  $T_{\text{NESS}}/T_E \approx 1.41$ . Units as in Fig. 6.

and 13. As the molecular structure of the fluid has not been taken into account in the long wavelength hydrodynamic approach of Sec. IV, the present theory cannot explain the structure in Figs. 10 and 13, and the structure factors predicted by the theory reach a plateau in the elastic regime ( $kl_0 \gtrsim \sqrt{\gamma_0}$ ), given by

$$\begin{aligned} S_{nn}(k) &\rightarrow n^2 T \chi_T, \\ S_{\alpha\beta}(\mathbf{k}) &\rightarrow \frac{T}{\rho} \delta_{\alpha\beta}, \end{aligned} \quad (46)$$

where  $\chi_T = (\partial n / \partial p)_T / n$  is the isothermal compressibility of the elastic hard disk fluid. For  $\alpha$  close to 1, the above limiting behavior is observed numerically for  $S_{ll}$  or  $S_{\perp}$ , and for  $S_{nn}$ , only in the limit of small packing fraction, where the molecular structure disappears.

When the inelasticity is increased, the structure factors exhibit the same  $k^{-2}$  behavior at large scale, but the theoretical expressions are less accurate (see Fig. 8). However, the theoretical curves are based on the Enskog estimate  $T_E$  for

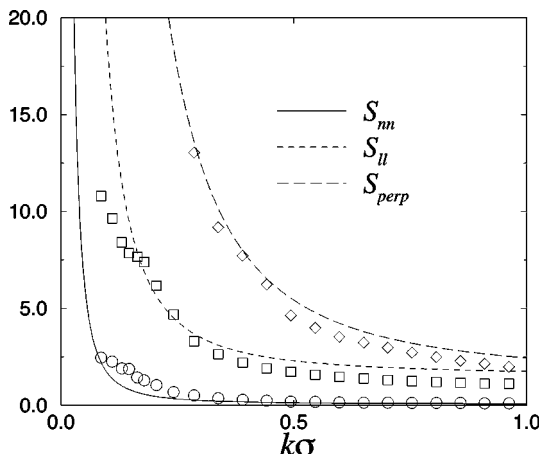


FIG. 9. Same as Fig. 8 where for the theoretical expressions (lines), the temperature has been set to the measured kinetic energy per particle,  $T \approx 1.45T_E$ .

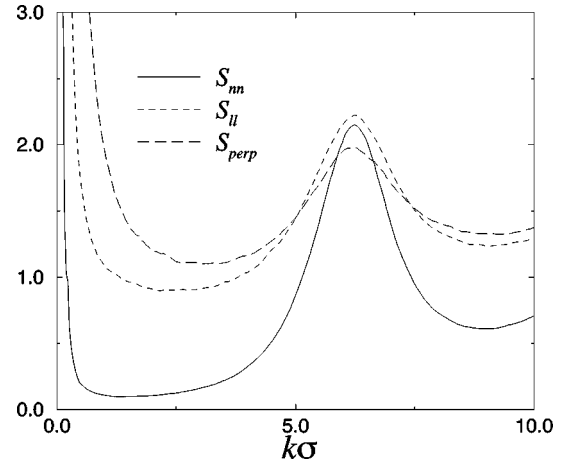


FIG. 10. Same as Fig. 8 beyond the dissipative regime. The theoretical structure factors are not displayed.

the granular temperature  $T$ , whereas for the system corresponding to Fig. 8,  $T \approx 1.45T_E$ . Our mode coupling theory predicts here  $T_{\text{NESS}} \approx 1.41T_E$ . Figure 9 displays the comparison between theory and simulation when the measured granular temperature is taken as an input for the hydrodynamic description. It appears that the large scale correlations (for which the present theory has been constructed) are well described by the theory, as long as the temperature is corrected from the mean-field Enskog prediction (10) to the measured value  $T$ . In the case of  $S_{\perp}$ , the amplitude only depends on the shear viscosity. The good agreement of the amplitude when the temperature is rescaled, while keeping for the shear viscosity the elastic hard disk value, suggests that the dependence of the shear viscosity on the inelasticity could be attributed only to the change in temperature. At the molecular scale,  $S_{ll}(k)$  and  $S_{\perp}(k)$  appear to be correlated to the density-density structure factor (see Fig. 10), in marked contrast to the elastic situation, where a plateau value would be reached. Such an effect is beyond the scope of our hydrodynamic approach, and is currently under investigation.

Surprisingly, in the case of complete inelasticity ( $\alpha = 0$ ), the theoretical structure factors give a reasonable pic-

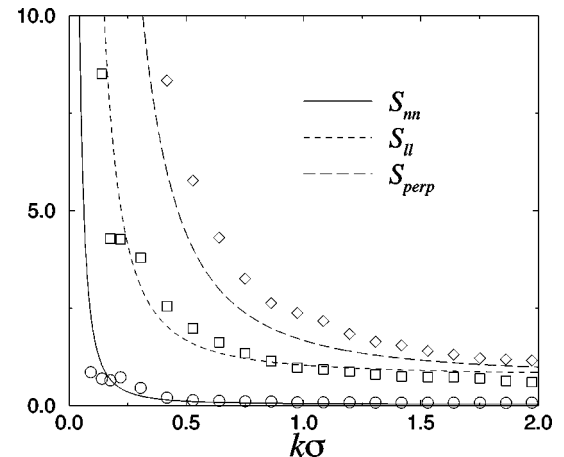


FIG. 11. Structure factors for  $\alpha=0$ ,  $\phi=0.63$ ,  $N=10201$ , and  $T_E=0.76T_0$ . Comparison is made with the hydrodynamic theory (lines). Here,  $T/T_E \approx 1.5$ , whereas mode coupling gives  $T_{\text{NESS}}/T_E \approx 1.77$ . Units as in Fig. 6.

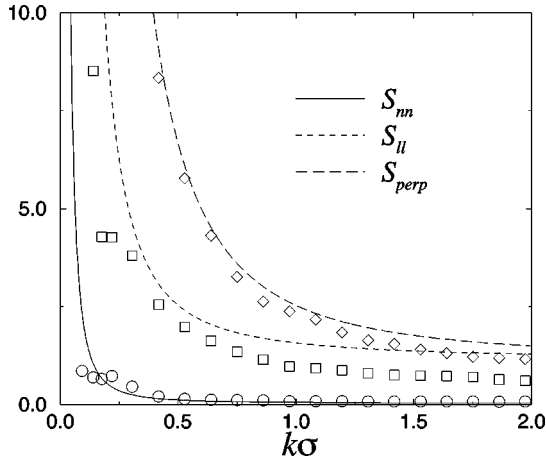


FIG. 12. Same as Fig. 11, where the simulation data (symbols) are compared to the theoretical predictions (lines) for which the temperature has been set to the measured kinetic energy per particle,  $T \approx 1.5T_E$ .

ture of the large wavelengths correlations in the fluid [especially for the longitudinal velocity component  $S_{\parallel}(k)$ , as shown in Fig. 11]. When the theoretical structure factors are deduced from the measured granular temperature  $T \approx 1.5T_E$  and not from  $T_E$  (our mode coupling theory predicts  $T_{\text{NESS}} \approx 1.77T_E$ ), the agreement for  $S_{\perp}(k)$  improves, but the mismatch for  $S_{\parallel}(k)$  increases (see Fig. 12). At small scales, the density correlations differ significantly from the elastic ones (Fig. 13) and the velocity structure factors exhibit the oscillatory behavior already present in Fig. 10, with peak positions locked in on the peaks in  $S_{nn}(k)$ . As can be expected from Figs. 11 and 12, the large scale correlations are compatible with the expected  $k^{-2}$  law (see Fig. 14) unlike the results of Peng and Ohta who report a  $k^{-1.4}$  asymptotic behavior for  $\alpha=0$ . However, a log-log plot such as Fig. 14 does not allow an accurate evaluation of the scaling exponents. The  $k^{-2}$  law is better inferred from the direct comparison with theory (Figs. 6,9,12).

Before concluding this section we compare the structure factors for the longitudinal flow fields, obtained from MD

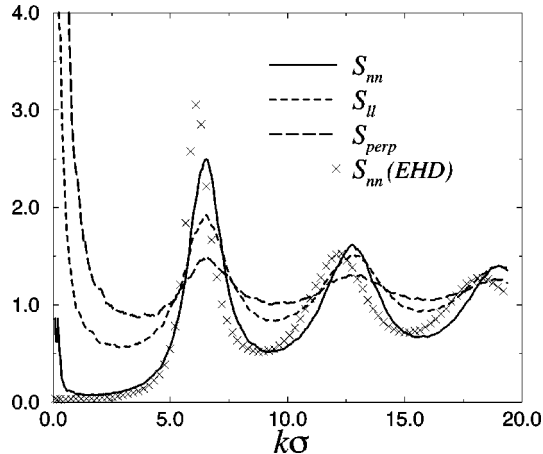


FIG. 13. Structure factors up to the molecular scale, for the same parameters as in Fig. 11.  $S_{nn}$  for elastic hard disks and the same packing fraction has also been plotted (crosses). Units as in Fig. 6.

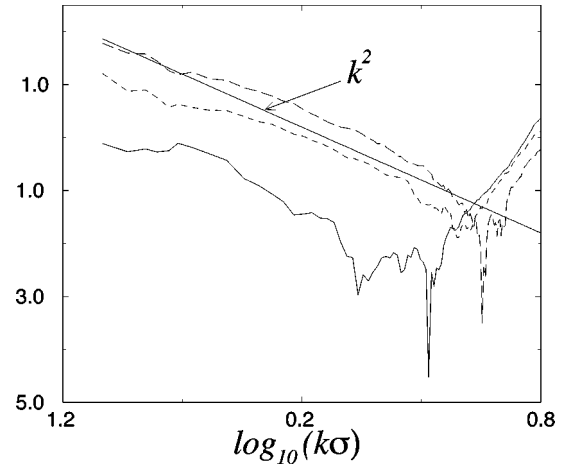


FIG. 14.  $\log_{10}|S - S_{\min}|$  versus  $\log_{10}(k\sigma)$ , for the same parameters as in Fig. 11. Here  $S_{\min}$  denotes the lowest value of structure factor  $S$ . The full, dashed, and long-dashed curves refer to  $S_{nn}$ ,  $S_{\parallel}$ , and  $S_{\perp}$ , respectively. Units as in Fig. 6.

simulations with two different theoretical predictions in Fig. 2, obtained by including or excluding internal noise. First, observe that all parameters in Fig. 2 and Fig. 6 are identical, as well as units on both axes. The simulation results for  $S_{\parallel}(k)$  in Fig. 6 are in excellent agreement with the theoretical prediction (dashed line), which corresponds to the solid line in Fig. 2 (internal plus external noise). The dotted line (without internal noise) for  $S_{\parallel}^{\text{without}}(k)$  in Fig. 2 disagrees with the simulations in the relevant interval  $0.2 \leq k\sigma \leq 0.5$ .

Hence, inclusion of internal noise extends the validity of the asymptotic theory to intermediate wave numbers.

## VIII. CONCLUSION

We have presented a theory for the large scale dynamics of a granular fluid that is driven into a nonequilibrium steady state by a random external force. Our description combines the macroscopic equations of motion for the hydrodynamic fields, accounting for energy dissipation through inelastic collisions and uniform heating, together with the fluctuating forces. The long-range character of the spatial correlation functions is determined by the small wave number divergence  $\sim k^{-2}$  of the corresponding structure factors. This  $k^{-2}$  behavior is typical for systems that combine conserving deterministic dynamics (conservation of particle number and momentum in collisions) with nonconserving noise [34], thus violating the fluctuation-dissipation condition, and is generic for rapid granular flows that are driven by external noise. We also draw attention to the analogy of our equations of motion for the fluctuating fields to the Edwards-Wilkinson model [35] that was proposed for growth of a granular surface. In that case the dynamic variable is a scalar field, namely, the height of the surface that obeys a similar equation of motion as any of the  $(d-1)$  components of the transverse velocity field,  $u_{\perp\alpha}(\mathbf{k}, t)$ , in our case. The only difference is that in the Edwards-Wilkinson model there is only nonconserving noise, whereas in our case both nonconserving (external) and conserving (internal) noise are present.

We have tested our predictions for the structure factors against molecular dynamics simulations and have demon-

strated that there is quantitative agreement over the whole wave-number range, if internal fluctuations are taken into account. In our two-dimensional simulations we have found deviations in the steady-state temperature and collision frequency that grow with the inelasticity and the system size. For not too large inelasticities ( $\alpha \geq 0.6$ ), we have explained these deviations in terms of mode coupling effects of the long-range fluctuations.

The phenomenological mode coupling theory, proposed in [20] and extended here to the driven IHS fluid, starts from the same basic ingredients as in the case of elastic fluids [36], where that theory was used to calculate the long-time tails of the velocity autocorrelation function and other current-current time correlation functions. For the elastic case the mode coupling theory can be derived from the *ring kinetic theory* in the low-density limit [37], which accounts for dynamic correlations built up by sequences of correlated binary collisions, leading to nonlocal effects in space and time. Such collision sequences correct the mean-field-type Boltzmann or Enskog kinetic equations for the errors induced by the breakdown of the molecular chaos assumption. The ring kinetic theory for rapid granular flows of IHS has been developed in Ref. [38], but has not yet been used to derive the present phenomenological mode coupling theory from the more fundamental kinetic theory, valid in the low-density limit.

In detailed balance models, such as elastic hard spheres, dynamic correlations created by correlated collision sequences lead to long-time tails, which imply that transport coefficients in two dimensions diverge as  $\ln L$  for large systems [36,37].

Nondetailed balance models, such as IHS fluids, generically exhibit long-range spatial correlations [19]. In randomly driven IHS fluids, as studied in this paper, these correlations between densities and flow fields at distant points in the fluid behave as  $1/r$  in 3D and  $\ln r$  in 2D, and already modify (renormalize) the mean-field Enskog-Boltzmann values for steady-state properties, such as the temperature and collision frequency. In 2D systems these renormalization corrections,  $\delta T$  and  $\delta \omega$ , exhibit the  $\ln L$  divergence, which in the case of detailed balance models appears only in the transport coefficients [19].

At larger inelasticity ( $\alpha \leq 0.6$ ), molecular chaos is also violated due to the presence of short-range velocity-velocity correlations (see Fig. 13), which are beyond our mode coupling theory. A detailed investigation of the small scale structure, which for large inelasticity clearly deviates from an equilibrium structure, will be reported in a subsequent publication. It is surprising that our description, which is based on the Enskog theory and neglects any dependence of transport coefficients on inelasticity, even at  $\alpha=0$  predicts the long-range structure reasonably well, provided that the temperature is not taken as the mean-field Enskog value, but set equal to the value measured in the simulations.

#### ACKNOWLEDGMENTS

The authors acknowledge useful discussions with D. Frenkel and I. Goldhirsch. E.T. and I.P. thank D. Frenkel and B. Mulder for the hospitality of their groups at AMOLF. T.v.N. and I.P. acknowledge support of the foundation

“Fundamenteel Onderzoek der Materie (FOM),” which is financially supported by the Dutch National Science Foundation (NWO).

#### APPENDIX A

In this appendix we derive expressions for the transport coefficients that govern the decay of fluctuations in the steady state. Linearization of the macroscopic equations (6) around the NESS, defined in Eqs. (9) and (10), gives the deterministic part of the following set of equations:

$$\begin{aligned} \partial_t \delta n &= -n \nabla \cdot \mathbf{u}, \\ \partial_t \mathbf{u} &= -\frac{1}{\rho} \nabla p + \nu \nabla^2 \mathbf{u} + (\nu_l - \nu) \nabla \nabla \cdot \mathbf{u} + \hat{\xi}, \\ \partial_t \delta T &= \frac{2\kappa}{dn} \nabla^2 \delta T - \frac{2p}{dn} \nabla \cdot \mathbf{u} - \delta \Gamma + \hat{\theta}. \end{aligned} \quad (\text{A1})$$

The noise terms  $\hat{\xi}(\mathbf{r}, t)$  and  $\hat{\theta}(\mathbf{r}, t)$  have been discussed in Sec. III. The pressure  $p$  is assumed to be that of EHS,  $p = nT(1 + \Omega_d \chi n \sigma^d / 2d)$ , where  $\Omega_d = 2\pi^{d/2} / \Gamma(d/2)$  is the  $d$ -dimensional solid angle, and  $\chi(n)$  is the equilibrium value of the pair-correlation function of EHS of diameter  $\sigma$  and mass  $m$  at contact. The kinematic and longitudinal viscosities  $\nu$  and  $\nu_l$ , as well as the heat conductivity  $\kappa$ , are also assumed to be approximately equal to the corresponding quantities for EHS, as calculated from the Enskog theory [22], where  $\rho\nu = \eta$  and  $\rho\nu_l = 2\eta(d-1)/d + \zeta$  are expressed in shear viscosity  $\eta$  and bulk viscosity  $\zeta$ . The collisional energy loss in Eq. (7),  $\Gamma = 2\gamma_0 \omega T$ , is proportional to the collision frequency

$$\omega = \Omega_d \chi n \sigma^{d-1} \sqrt{\frac{T}{\pi m}}, \quad (\text{A2})$$

as obtained from the Enskog theory. In two dimensions we use the Verlet-Levesque approximation  $\chi = (1 - 7\phi/16)/(1 - \phi)^2$ .

By taking spatial Fourier transforms  $\delta a(\mathbf{k}, t) = \int d\mathbf{r} \delta a(\mathbf{r}, t) \exp(-i\mathbf{k} \cdot \mathbf{r})$  in Eqs. (A1), one obtains the mesoscopic equation (18) with the hydrodynamic matrix

$\mathbf{M}(\mathbf{k})$

$$= - \begin{pmatrix} 0 & 0 & ikn & 0 \\ \gamma_0 \omega g(n) T/n & 3\gamma_0 \omega + D_T k^2 & ik2p/dn & 0 \\ ikv_T^2/n & ikp/\rho T & \nu_l k^2 & 0 \\ 0 & 0 & 0 & \nu k^2 \end{pmatrix}. \quad (\text{A3})$$

It contains the coefficients

$$\begin{aligned} g(n) &= 2 \left( 1 + \frac{n}{\chi} \frac{d\chi}{dn} \right), \\ v_T^2 &= \left( \frac{\partial p}{\partial \rho} \right)_T, \end{aligned} \quad (\text{A4})$$

$$D_T = \frac{2\kappa}{dn}.$$

In the body of the paper we need the eigenvalues  $z_\lambda(\mathbf{k})$  of the asymmetric matrix  $M_{ab}(\mathbf{k})$ , and its right and left eigenvectors, which are obtained from

$$\begin{aligned} \mathbf{M}(\mathbf{k})\mathbf{w}_\lambda(\mathbf{k}) &= z_\lambda(\mathbf{k})\mathbf{w}_\lambda(\mathbf{k}), \\ \mathbf{M}^T(\mathbf{k})\mathbf{v}_\lambda(\mathbf{k}) &= z_\lambda(\mathbf{k})\mathbf{v}_\lambda(\mathbf{k}), \end{aligned} \quad (\text{A5})$$

where  $\mathbf{M}^T$  is the transpose of  $\mathbf{M}$ . Here  $\lambda = \pm$  labels the sound modes,  $\lambda = H$  labels the heat mode, and  $\lambda = \perp$  labels  $(d-1)$  degenerate shear or transverse velocity modes. The eigenvectors form a complete biorthonormal basis, i.e.,

$$\begin{aligned} \sum_a v_{\lambda a}(\mathbf{k}) w_{\mu a}(\mathbf{k}) &\equiv \langle \mathbf{v}_\lambda | \mathbf{w}_\mu \rangle = \delta_{\lambda\mu}, \\ \sum_\lambda |\mathbf{w}_\lambda(\mathbf{k})\rangle \langle \mathbf{v}_\lambda(\mathbf{k})| &= \mathbf{I}. \end{aligned} \quad (\text{A6})$$

Moreover, the eigenvalue equation,  $\det[z(k)\mathbf{I} - \mathbf{M}(\mathbf{k})] = 0$ , is an *even* function of  $\mathbf{k}$ . Consequently,  $\mathbf{M}(\mathbf{k})$  and  $\mathbf{M}(-\mathbf{k})$  have the same eigenvalues, which are either real or form a complex conjugate pair. So we choose  $z_\lambda(\mathbf{k}) = z_\lambda(-\mathbf{k}) = z_\lambda(k)$ . The corresponding eigenvectors of  $\mathbf{M}(-\mathbf{k})$  in case of the sound modes are obtained from the transformation  $\{\mathbf{w}_+(-\mathbf{k}), \mathbf{v}_+(-\mathbf{k})\} \leftrightarrow \{\mathbf{w}_-(\mathbf{k}), \mathbf{v}_-(\mathbf{k})\}$ . All other eigenvectors are invariant under the transformation  $\mathbf{k} \rightarrow -\mathbf{k}$ .

By setting  $z(k) = 0$  in the eigenvalue equation, one can verify that there are no zero crossings at any finite wave number. So, all eigenvalues have a definite (here *negative*) sign. Consequently, all modes of the heated IHS fluid are linearly stable. There is *no* clustering instability [23,28] and *no* instability in the flow field [23], as in the freely evolving IHS fluid.

In the *dissipative regime* ( $kl_0 \ll \gamma_0$ ), the eigenvalue equation is solved by an expansion in powers of  $k$ , and one finds to dominant orders the eigenvalues in the form (25) and eigenvectors in the form (26). The eigenmodes to dominant nonvanishing order in  $k$  are listed in Eq. (26). There are  $(d-1)$  transverse velocity or shear modes ( $\lambda = \perp$ ), which are purely diffusive with a diffusivity  $D_\perp = \nu$ ; there are two propagating modes ( $\lambda = \pm$ ) with a speed of propagation  $v_D$ , and sound damping constant  $D_S$ , and a *kinetic* heat mode ( $\lambda = H$ ) with a nonvanishing  $z_H(0)$ .

For later reference we also express these coefficients in thermodynamic quantities and transport coefficients. The speed of sound  $v_D$  in the *dissipative regime* ( $kl_0 \ll \gamma_0$ ) is

$$v_D^2 = \left( \frac{\partial p}{\partial \rho} \right)_T - \frac{2p}{3\rho} \left( 1 + \frac{n}{\chi} \frac{d\chi}{dn} \right). \quad (\text{A7})$$

It satisfies the inequality  $v_D < v_S$ , where  $v_S$  is the adiabatic speed of sound in the *standard regime* ( $\gamma_0 \ll kl_0 < 1$ ),

$$v_S^2 = v_T^2 + \left( \frac{2p}{dn} \right) \left( \frac{p}{\rho T} \right) = \left( \frac{\partial p}{\partial \rho} \right)_S. \quad (\text{A8})$$

The damping constant of the sound modes is

$$D_S = \frac{1}{2} v_l + \frac{p}{9\gamma_0\omega\rho} \left( 1 + \frac{n}{\chi} \frac{d\chi}{dn} + \frac{3p}{dnT} \right), \quad (\text{A9})$$

and the dispersion relation for the kinetic heat mode contains the positive constant

$$D_H = -\frac{2\kappa}{dn} + \frac{2p}{9\gamma_0\omega\rho} \left( 1 + \frac{n}{\chi} \frac{d\chi}{dn} + \frac{3p}{dnT} \right). \quad (\text{A10})$$

The ratios  $v_D^2/T$ ,  $v_S^2/T$ ,  $D_S/\sqrt{T}$ , and  $D_H/\sqrt{T}$  are independent of temperature.

## APPENDIX B

In this appendix we calculate the tails of the spatial correlation functions  $G_{ab}(\mathbf{r})$ , which is done by Fourier inversion of  $S_{ab}(\mathbf{k})$ . Consider first the tensor fields  $G_{\alpha\beta}(\mathbf{r})$  and  $S_{\alpha\beta}(\mathbf{k})$  in Eq. (1) with  $\delta a_\alpha(\mathbf{r}, t) = u_\alpha(\mathbf{r}, t)$  ( $\alpha, \beta = x, y, \dots$ ) being the components of the flow field. Both tensor fields are isotropic and can be split into longitudinal and transverse components, i.e.,

$$\begin{aligned} G_{\alpha\beta}(\mathbf{r}) &= \hat{r}_\alpha \hat{r}_\beta G_{\parallel}(r) + (\delta_{\alpha\beta} - \hat{r}_\alpha \hat{r}_\beta) G_{\perp}(r) \\ &= \int \frac{d\mathbf{k}}{(2\pi)^d} \exp(i\mathbf{k} \cdot \mathbf{r}) [\hat{k}_\alpha \hat{k}_\beta S_{\parallel}(k) \\ &\quad + (\delta_{\alpha\beta} - \hat{k}_\alpha \hat{k}_\beta) S_{\perp}(k)], \end{aligned} \quad (\text{B1})$$

where the small- $k$  behavior of  $S_{\perp}(k)$  and  $S_{\parallel}(k)$  is given in Eqs. (27) and (28). By contracting the second line above with  $\hat{r}_\alpha \hat{r}_\beta$ , we obtain

$$\begin{aligned} G_{\parallel}(r) &= \int \frac{d\mathbf{k}}{(2\pi)^d} \exp(i\mathbf{k} \cdot \mathbf{r}) [(\hat{\mathbf{k}} \cdot \hat{\mathbf{r}})^2 S_{\parallel}(k) \\ &\quad + [1 - (\hat{\mathbf{k}} \cdot \hat{\mathbf{r}})^2] S_{\perp}(k)]. \end{aligned} \quad (\text{B2})$$

Contraction of the second line of Eq. (B1) with  $(\delta_{\alpha\beta} - \hat{k}_\alpha \hat{k}_\beta)$  yields in a similar manner an expression for  $G_{\perp}(r)$ .

In *three* dimensions the  $\mathbf{k}$  integral can be performed explicitly and yields

$$\int \frac{d\mathbf{k}}{(2\pi)^3} \frac{\exp(i\mathbf{k} \cdot \mathbf{r})}{k^2} = \frac{1}{4\pi r}, \quad (\text{B3})$$

$$\int \frac{d\mathbf{k}}{(2\pi)^3} \frac{\exp(i\mathbf{k} \cdot \mathbf{r})}{k^2} (\hat{\mathbf{k}} \cdot \hat{\mathbf{r}})^2 = 0.$$

The resulting large- $r$  behavior of  $G_{\alpha\beta}(\mathbf{r})$  is given in Eqs. (30).

In *two* dimensions the integral in Eq. (B2) over the azimuthal angle yields for large  $r$ ,

$$\begin{aligned} \int \frac{d\mathbf{k}}{(2\pi)^2} \frac{\exp(i\mathbf{k} \cdot \mathbf{r})}{k^2} &= \frac{1}{2\pi} \int_{k_{\min}}^{\infty} \frac{dk}{k} J_0(kr) \\ &\simeq \frac{1}{2\pi} \ln \left( \frac{L}{r} \right) + \mathcal{O}(1), \end{aligned}$$

$$\begin{aligned} & \int \frac{d\mathbf{k}}{(2\pi)^2} \frac{\exp(i\mathbf{k}\cdot\mathbf{r})}{k^2} [1 - (\hat{\mathbf{k}}\cdot\hat{\mathbf{r}})^2] \\ &= \frac{1}{2\pi r} \int_{k_{\min}}^{\infty} \frac{dk}{k^2} J_1(kr) \approx \frac{1}{4\pi} \ln\left(\frac{L}{r}\right) + \mathcal{O}(1). \end{aligned} \quad (\text{B4})$$

In two dimensions the  $\mathbf{k}$  integral diverges for  $k \rightarrow 0$ . It should, in fact, be restricted to  $k \geq k_{\min} = 2\pi/L$ , which is the smallest allowed wave number when periodic boundary conditions are imposed. To obtain the last equalities one needs the small- $z$  behavior of the Bessel functions  $J_\nu(z) \approx (z/2)^\nu / \Gamma(\nu + 1)$  [39]. Combining these results with Eq. (B2) yields for large  $r$ ,

$$G_{\parallel}(r) \approx G_{\perp}(r) \approx \frac{\Gamma}{8\pi\rho} \left( \frac{1}{\nu} + \frac{1}{2D_S} \right) \ln\left(\frac{L}{r}\right). \quad (\text{B5})$$

The remaining spatial correlation functions  $G_{ab}(r)$  involving  $a, b = \{n, T\}$ , are scalar fields. Their large- $r$  behavior is given by

$$\begin{aligned} G_{ab}(r) &= \int \frac{d\mathbf{k}}{(2\pi)^d} \exp(i\mathbf{k}\cdot\mathbf{r}) S_{ab}(k) \\ &= \frac{\Gamma B_{ab}}{8\pi\rho D_S} \begin{cases} \ln(L/r) & (d=2) \\ 1/2r & (d=3), \end{cases} \end{aligned} \quad (\text{B6})$$

where  $B_{ab}(k)$  is given in Table I. The subleading corrections of  $\mathcal{O}(r^0)$  depend on the cutoff  $k_{\min}$ . To evaluate these terms requires the subleading small- $k$  behavior of  $S_{ab}(k)$  in Eqs. (27) to (29).

### APPENDIX C

In this appendix we present a mode coupling calculation to estimate the contributions of the long wavelength fluctuations in the NESS to some quantity  $h$ . Examples are the particle distribution functions, the energy per particle  $E$ , and the collision frequency  $\omega$ . The fluctuations are correlated over large distances, as a consequence of sequences over dynamically correlated collisions, the so-called ring collisions [40], as shown in Sec. V by explicit calculation of their spatial tails.

To calculate their contributions to average quantities like  $h$ , one may solve the ring kinetic equations [38], or estimate these quantities from a more phenomenological mode coupling approach, as developed in Ref. [36]. The basic assumption made there is that the state of the system rapidly decays to a state of local equilibrium, described by the fluctuating hydrodynamic fields  $\mathbf{a}(\mathbf{r}, t) = \{n(\mathbf{r}, t), u_\alpha(\mathbf{r}, t), T(\mathbf{r}, t)\}$ .

For the quantity under consideration this can be implemented by representing  $h = (1/V) \int d\mathbf{r} h(\mathbf{r})$ , and approximating  $h(\mathbf{r})$  by its value in local equilibrium, i.e.,

$$h_{\text{NESS}} = \frac{1}{V} \int d\mathbf{r} \langle h_l(\mathbf{a}(\mathbf{r})) \rangle, \quad (\text{C1})$$

where the average is taken over the fluctuating hydrodynamic fields  $\mathbf{a}(\mathbf{r})$  in the NESS. To carry out the average over

the fluctuations, we expand  $h_l(\mathbf{a})$  in powers of the fluctuations  $\delta a = a - \langle a \rangle$  around the NESS, yielding

$$\begin{aligned} h_{\text{NESS}} &\approx h_l(\langle \mathbf{a} \rangle) + \frac{1}{2V} \int d\mathbf{r} \langle \delta a(\mathbf{r}) \delta b(\mathbf{r}) \rangle A_{ab} \\ &= h_l(\langle \mathbf{a} \rangle) + \frac{1}{2} \int \frac{d\mathbf{k}}{(2\pi)^d} S_{ab}(k) A_{ab}, \end{aligned} \quad (\text{C2})$$

where summation convention for repeated indices has been used. Here  $A_{ab}$  is the matrix of second derivatives  $\partial^2 h_l(\mathbf{a}) / \partial \mathbf{a} \partial \mathbf{a}$  at  $\mathbf{a} = \langle \mathbf{a} \rangle$ . The asterisk indicates that  $\mathbf{k}$  integrals are restricted to the long wavelength range,  $k < \gamma_0/l_0$ , the so-called dissipative range, discussed below (16). In this range the structure factors have the form  $S_{ab}(k) \approx E_{ab}/k^2$  on account of Eqs. (27) to (29).

For dimensionality  $d \geq 3$  the fluctuation contribution  $\delta h = h_{\text{NESS}} - h_l(\langle \mathbf{a} \rangle)$  is convergent at small  $k$ , and gives only small well-behaved corrections to  $h_l(\langle \mathbf{a} \rangle)$ . However, for  $d = 2$ , the  $\mathbf{k}$  integral diverges logarithmically at small  $k$  (where  $k \geq 2\pi/L$ ), and the excess  $\delta h$  is given by

$$\delta h \approx \frac{A_{ab} E_{ab}}{4\pi} \int_{2\pi/L}^{\gamma_0/l_0} \frac{dk}{k} \approx \frac{A_{ab} E_{ab}}{4\pi} \ln\left(\frac{\gamma_0 L}{l_0}\right). \quad (\text{C3})$$

Consequently, the fluctuation contribution  $\delta h$  in 2D systems is a singular function of the system size  $L$  that diverges in the thermodynamic limit.

We first apply the above results to the energy per particle,  $E = (1/N) \int d\mathbf{r} e_l(\mathbf{a}(\mathbf{r}))$ , where  $e_l(\mathbf{a}) = \frac{1}{2} \rho u^2 + (d/2) n T$  is the energy density in local equilibrium. From  $e_l(\mathbf{a})$ , the expansion coefficients corresponding to  $h_l(\langle \mathbf{a} \rangle)$  and  $A_{ab}$  in Eq. (C2) can be calculated, to yield in  $d = 2$ :

$$\delta E \approx \frac{1}{2n} \int \frac{d\mathbf{k}}{(2\pi)^2} [\rho S_{\perp}(k) + \rho S_{ll}(k) + 2S_{nT}(k)]. \quad (\text{C4})$$

Inserting Eq. (27) to (29) then yields

$$\delta E \approx \frac{\gamma_0 \omega_E T_E}{4\pi n} \left[ \frac{1}{\nu} + \frac{1}{2D_S} \left( 1 + \frac{2B_{nT}}{\rho} \right) \right] \ln\left(\frac{\gamma_0 L}{l_0}\right), \quad (\text{C5})$$

where the coefficient  $B_{nT}$  is listed in Table I.

For the collision frequency the analog of Eq. (C1) is  $\omega = (1/N) \int d\mathbf{r} \langle n(\mathbf{r}) \omega_l(\mathbf{a}(\mathbf{r})) \rangle$  with  $\omega_l(\mathbf{a}) \propto n \chi(n) \sqrt{T}$  given in Eq. (A2). This gives in two dimensions:

$$\begin{aligned} \delta \omega &\approx \frac{1}{2n} \int \frac{d\mathbf{k}}{(2\pi)^2} [S_{nn}(k) A_{nn} + 2S_{nT}(k) A_{nT} + S_{TT}(k) A_{TT}] \\ &\approx \frac{\gamma_0 \omega_E T_E}{8\pi n \rho D_S} [B_{nn} A_{nn} + 2B_{nT} A_{nT} + B_{TT} A_{TT}] \ln\left(\frac{\gamma_0 L}{l_0}\right), \end{aligned} \quad (\text{C6})$$

where the coefficients  $B_{ab}$  are given in Table I, and  $A_{nn} = \partial^2(n\omega) / \partial n^2$ ,  $A_{nT} = \partial^2(n\omega) / \partial n \partial T$ , and  $A_{TT} = \partial^2(n\omega) / \partial T^2$  at  $\mathbf{a} = \langle \mathbf{a} \rangle$ .

The same method can be used to calculate other averages, as well as particle distribution functions. For instance, for the single-particle distribution function, the starting point would be

$$f_{\text{NESS}}(\mathbf{v}) = (1/V) \int d\mathbf{r} \langle f_i(\mathbf{v} | \mathbf{a}(\mathbf{r})) \rangle, \quad (\text{C7})$$

and the above procedure can be applied at once.

- 
- [1] H. M. Jaeger, S. R. Nagel, and R. P. Behringer, *Rev. Mod. Phys.* **68**, 1259 (1996).
- [2] R. A. Bagnold, *Proc. R. Soc. London, Ser. A* **225**, 49 (1954).
- [3] S. B. Savage and M. Sayed, *J. Fluid Mech.* **142**, 391 (1984).
- [4] P. C. Johnson, P. Nott, and R. Jackson, *J. Fluid Mech.* **210**, 501 (1990).
- [5] S. Warr, J. M. Huntley, and G. T. H. Jacques, *Phys. Rev. E* **52**, 5583 (1995).
- [6] F. Melo, P. B. Umbanhowar, and H. L. Swinney, *Phys. Rev. Lett.* **75**, 3838 (1995).
- [7] L. S. Tsimring and I. S. Aranson, *Phys. Rev. Lett.* **79**, 213 (1997); D. H. Rothman, *Phys. Rev. E* **57**, R1239 (1998); S. C. Venkataramani and E. Ott, *Phys. Rev. Lett.* **80**, 3495 (1998).
- [8] M. Cross and P. C. Hohenberg, *Rev. Mod. Phys.* **65**, 851 (1993).
- [9] A. Kudrolli, M. Wolpert, and J. P. Gollub, *Phys. Rev. Lett.* **78**, 1383 (1997).
- [10] J. S. Olafsen and J. S. Urbach, *Phys. Rev. Lett.* **81**, 4369 (1998).
- [11] J. T. Jenkins and M. W. Richman, *Arch. Ration. Mech. Anal.* **87**, 355 (1985); J. J. Brey, J. W. Dufty, and A. Santos, *J. Stat. Phys.* **87**, 1051 (1997); N. Sela and I. Goldhirsch, *J. Fluid Mech.* **361**, 41 (1998).
- [12] D. R. Williams and F. C. MacKintosh, *Phys. Rev. E* **54**, R9 (1996).
- [13] G. Peng and T. Ohta, *Phys. Rev. E* **58**, 4737 (1998).
- [14] L. Oger, C. Annic, D. Bideau, R. Dai, and S. B. Savage, *J. Stat. Phys.* **82**, 1047 (1996).
- [15] R. Jackson, in *Fluidization*, edited by J. F. Davidson, R. Clift, and D. Harrison (Academic Press, London, 1985).
- [16] C. Bizon and H. L. Swinney (private communication).
- [17] T. P. C. van Noije and M. H. Ernst, *Granular Matter* **1**, 57 (1998).
- [18] M. R. Swift, M. Boamfa, S. J. Cornell, and A. Maritan, *Phys. Rev. Lett.* **80**, 4410 (1998).
- [19] J. R. Dorfman, T. R. Kirkpatrick, and J. Sengers, *Annu. Rev. Phys. Chem.* **45**, 213 (1994).
- [20] R. Brito and M. H. Ernst, *Europhys. Lett.* **43**, 497 (1998).
- [21] J. P. Hansen and I. R. McDonald, *Theory of Simple Liquids* (Academic Press, London, 1986).
- [22] S. Chapman and T. G. Cowling, *The Mathematical Theory of Non-uniform Gases* (Cambridge University Press, Cambridge, 1970).
- [23] T. P. C. van Noije, M. H. Ernst, R. Brito, and J. A. G. Orza, *Phys. Rev. Lett.* **79**, 411 (1997); T. P. C. van Noije, R. Brito, and M. H. Ernst, *Phys. Rev. E* **57**, R4891 (1998).
- [24] U. Frisch, B. Hasslacher, and Y. Pomeau, *Phys. Rev. Lett.* **56**, 1505 (1986).
- [25] D. H. Rothman and S. Zaleski, *Rev. Mod. Phys.* **66**, 1417 (1994).
- [26] S. McNamara, *Phys. Fluids A* **5**, 3056 (1993).
- [27] L. Landau and E. M. Lifshitz, *Fluid Mechanics* (Pergamon Press, New York, 1959), Chap. 17.
- [28] I. Goldhirsch and G. Zanetti, *Phys. Rev. Lett.* **70**, 1619 (1993).
- [29] S. McNamara and W. R. Young, *Phys. Fluids A* **4**, 496 (1992); *Phys. Rev. E* **50**, R28 (1994); **53**, 5089 (1996).
- [30] P. Deltour and J.-L. Barrat, *J. Phys. I* **7**, 137 (1997).
- [31] A. Puglisi, V. Loreto, U. Marini Bettolo Marconi, A. Petri, and A. Vulpiani, *Phys. Rev. Lett.* **81**, 3848 (1998).
- [32] M. P. Allen and D. J. Tildesley, *Computer Simulations of Liquids* (Clarendon Press, Oxford, 1987).
- [33] S. Jasty, M. Al-Naghy, and M. de Llano, *Phys. Rev. A* **35**, 1376 (1987).
- [34] G. Grinstein, D.-H. Lee, and S. Sachdev, *Phys. Rev. Lett.* **64**, 1927 (1990).
- [35] S. F. Edwards and D. R. Wilkinson, *Proc. R. Soc. London, Ser. A* **381**, 17 (1982).
- [36] M. H. Ernst, E. H. Hauge, and J. M. J. van Leeuwen, *Phys. Rev. Lett.* **25**, 1245 (1970); *Phys. Rev. A* **4**, 2055 (1971).
- [37] J. R. Dorfman and E. G. D. Cohen, *Phys. Rev. Lett.* **25**, 1257 (1970); M. H. Ernst and J. R. Dorfman, *Physica (Amsterdam)* **61**, 157 (1972).
- [38] T. P. C. van Noije, M. H. Ernst, and R. Brito, *Physica A* **251**, 266 (1998).
- [39] I. S. Gradshteyn and I. M. Ryzhik, *Table of Integrals, Series, and Products* (Academic Press, New York, 1965).
- [40] J. R. Dorfman and H. van Beijeren, in *Statistical Mechanics, Part B: Time-Dependent Processes*, edited by B. J. Berne (Plenum Press, New York, 1977), Chap. 3.